
Article:
Schwendike, J, Jones, SC, Vogel, B et al. (2016) Mineral dust transport toward Hurricane Helene (2006). Journal of Geophysical Research: Atmospheres, 121 (10). pp. 5538-5566. ISSN: 2169-897X

https://doi.org/10.1002/2015JD024708

AGU PUBLICATIONS

JGR

Journal of Geophysical Research: Atmospheres

RESEARCH ARTICLE

10.1002/2015JD024708

Mineral dust transport toward Hurricane Helene (2006)

Juliane Schwendike[1,2,3], Sarah C. Jones[1,4], Bernhard Vogel[1], and Heike Vogel[1]

[1]Institute for Meteorology and Climate Research (IMK-TRO), Karlsruhe Institute of Technology, Karlsruhe, Germany, [2]School of Earth, Atmosphere and Environment, Monash University, Clayton, Victoria, Australia, [3]School of Earth and Environment, University of Leeds, Leeds, UK, [4]Deutscher Wetterdienst, Frankfurter Straße 135, Offenbach, Germany

Key Points:
- Dust-enriched air can be dry or moist
- Dusty air can become trapped in the AEW trough
- Upward dust transport by convection, at coastal baroclinic zone, and at ITD

Correspondence to:
J. Schwendike,
j.schwendike@leeds.ac.uk

Citation:
Schwendike, J., S. C. Jones, B. Vogel, and H. Vogel (2016), Mineral dust transport toward Hurricane Helene (2006), *J. Geophys. Res. Atmos.*, *121*, 5538–5566, doi:10.1002/2015JD024708.

Received 4 JAN 2016
Accepted 26 MAR 2016
Accepted article online 31 MAR 2016
Published online 28 MAY 2016

Abstract This study investigates the transport of mineral dust from its source regions in West Africa toward the developing tropical cyclone Helene (2006) and diagnoses the resulting properties of the air influencing the tropical cyclonegenesis. The model system COSMO-ART (Consortium for Small-Scale Modelling-Aerosols and Reactive Trace gases) in which the emission and transport of mineral dust as well as the radiation feedback are taken into account, was used. The emission of mineral dust between 9 and 14 September 2006 occurred in association with the relatively strong monsoon flow and northeasterly trade winds, with gust fronts of convective systems over land, and with the Atlantic inflow. Additionally, increased surface wind speed was linked to orographical effects at the Algerian Mountains, Atlas Mountains, and the Hoggar. The dust, as part of the Saharan air layer, is transported at low levels by the monsoon flow, the Harmattan, the northeasterly trade winds, and the monsoon trough, and is transported upward in the convergence zone between Harmattan and monsoon flow, in the baroclinic zone along the West African coastline, and by convection. At around 700 hPa the dust is transported by the African easterly jet. Dry and dust-free air is found to the north-northwest of the developing tropical depression due to descent in an anticyclone. Based on the model data, it was possible to distinguish between dry (from the anticyclone), dry and dusty (from the Harmattan and northeasterly trade winds), and dusty and moist air (from the monsoon flow and in the tropical depression due to convection).

1. Introduction

The region south of the Cape Verde islands in the eastern Atlantic is a key location for tropical cyclogenesis. Tropical cyclones forming in this region are subject to a variety of environmental influences emanating from the West African Monsoon system, the Saharan planetary boundary layer, and subtropical circulation features. These environmental influences determine the properties of the air in and around a developing tropical cyclone and, in particular, its moisture and mineral dust content. It is not yet fully understood how these properties influences the genesis and intensity of tropical cyclones. Assessing the role of mineral dust in tropical cyclogenesis and storm intensity is thus a crucial step to improve our forecast ability. In order to be able to investigate the impact of mineral dust on tropical cyclones it is essential to diagnose where the air in the storm and in the vicinity of the storm is coming from and how it is characterized.

Dunion and Velden [2004] were among the first to suggest a relation between tropical cyclone intensity change and the Saharan air layer (SAL). The SAL consists of the elevated Saharan planetary boundary layer which occurs at the height of the African easterly jet (AEJ) with the monsoon flow underneath it and the free atmosphere aloft, and the well-mixed layer above the Saharan desert reaching from the surface up to about 500 hPa. It is characterized by a significant amount of mineral dust aerosols, relatively dry and warm air, and a weakly stable stratification [*Prospero and Carlson*, 1972; *Carlson and Prospero*, 1972; *Diaz et al.*, 1976; *Karyampudi and Carlson*, 1988; *Parker et al.*, 2005a]. The SAL can be transported across the Atlantic and into the Caribbean conserving its thermodynamic structure [*Carlson and Prospero*, 1972]. The temperature inversion typically found at the SAL's base may contribute to the longevity of this dry air [*Dunion and Velden*, 2004]. Maximum dust concentrations occur near the AEJ axis at about 650 hPa with downward extension of heavy dust into the marine boundary layer and a relatively dust-free trade wind inversion layer to the north of the dust layer over the eastern Atlantic region [*Karyampudi et al.*, 1999]. The dry air over the eastern Atlantic below about 600 hPa is mainly due to the SAL. Between about 600 and 400 hPa, the deep dry convective mixing over the Sahara leads to a moistening and a slight cooling effect relative to the very dry ambient air at the

middle and upper levels in the region. The dry air over the eastern and subtropical Atlantic is partly a result of large-scale descent on the eastern side of the Azores high-pressure system [*Braun*, 2010].

Dunion and Velden [2004] propose the following three mechanisms by which the SAL can inhibit the formation or reduce the intensity of tropical cyclones in the North Atlantic. (i) Convectively driven downdrafts are enhanced by dry air at middle levels, which leads to stronger evaporation and thus a cooling of the planetary boundary layer and hence to a weakening of the tropical cyclone. (ii) The AEJ, which can be found at the southern boundary of the SAL, increases the local vertical wind shear. This shear can decouple the storm's low-level circulation from its supporting middle and upper level deep convection. (iii) The radiative effects of mineral dust in the SAL may enhance the preexisting trade wind inversion and act to stabilize the environment and hence suppress deep convection [see, e.g., *Carlson and Benjamin*, 1980; *Wong and Dessler*, 2005; *Jones et al.*, 2007; *Zhang et al.*, 2007; *Sun et al.*, 2009].

In contrast, AEW growth and thus the potential for tropical cyclogenesis can be related to the SAL [*Karyampudi and Carlson*, 1988; *Karyampudi et al.*, 1999; *Karyampudi and Pierce*, 2002]. The SAL is important for the growth and maintenance of some AEWs due to a stronger meridional circulation and greater latent heat release in cumulus convection due to stronger baroclinity along the lateral boundary of the SAL. Additionally, the SAL increases the strength of the AEJ which leads to weak or negative potential vorticity north of the AEJ and positive potential vorticity south of it. The enhanced horizontal potential vorticity gradient amplifies the growth of the wave due to barotropic instability.

Dust emission over West Africa can occur in association with a variety of different weather systems. One mechanism for dust emission over North Africa is the penetration of upper level troughs to low latitudes [*Knippertz and Fink*, 2006]. Dust emission is also linked to increased surface wind speed caused by, e.g., density currents associated with strong evaporational cooling along precipitating cloud bands over the northern Sahara [*Knippertz and Fink*, 2006] and along the Saharan side of the Atlas Mountain chain in southern Morocco [*Knippertz et al.*, 2007]. The density currents due to mesoscale convective systems (MCSs) are very effective for the emission of dust and its injection to altitudes favorable for long-range transport. This process is of particular importance at the beginning of the monsoon season, before the growing vegetation rapidly inhibits local dust emission [*Flamant et al.*, 2007], and when greater energy is available to the downdrafts from the convective systems [*Marsham et al.*, 2008]. Additionally, dust uplift is associated with density currents at the leading edge of the Atlantic inflow [*Grams et al.*, 2010].

A strong density gradient occurs across the monsoon-Harmattan interface, due to the temperature and humidity differences between the monsoon and Harmattan flow. Large dust uplifts are caused by strong low-level jets north of the Intertropical Discontinuity (ITD), in the morning hours just after sunrise [*Bou Karam et al.*, 2008]. South of the ITD, the emission of mineral dust occurs during the night and in the early morning hours before sunrise. The circulation in the head of the monsoon density current lifts the mobilized dust rearward along an isentropic surface. The stable stratification north of the ITD prevents the dust from reaching altitudes at which it could be transported over long distances by the Harmattan. Later in the day turbulent mixing throughout the planetary boundary layer takes place, and the dust is transported southward by the Harmattan [*Bou Karam et al.*, 2008]. The ITD acts to raise the mineral dust layer over the southwesterly monsoon flow into the AEJ core [*Flamant et al.*, 2009], and the AEJ transports the dust across West Africa and the Atlantic.

To understand the effect of mineral dust on tropical cyclogenesis and the intensity changes of tropical cyclones, it is crucial to know where the dust occurs relative to the storm and how it got there. Therefore, this study investigates the pathways and characteristics of air in the vicinity and in the center of the developing tropical cyclone that later became Hurricane Helene between 9 and 14 September 2006. During the study period Helene intensified from a 13 m s^{-1} (25 kn) tropical depression to a 60 m s^{-1} (117 kn) category 3 hurricane, and large amounts of mineral dust were being emitted and transported across West Africa and the Atlantic. This time was also coincident with the special observation period of the African Monsoon Multidisciplinary Analyses (AMMA) project [*Redelsperger et al.*, 2006].

The aim of the present study is to show where the dust laden and the dry air are located relative to the developing tropical depression that became Hurricane Helene. The new aspect of this study is to show how the mineral dust is transported from its source regions toward the storm and that dust can occur in both dry and moist conditions. Based on model simulations trajectories are calculated to determine where the air in the

center and in the vicinity of Helene originates. Additionally, the model data allows the differences between dry air, dry, and dusty air, as well as dusty and moist air to be distinguished. Hence, in this study we are going to address the following question: How is the mineral dust transported from its source regions to the developing tropical storm and what are the implications of this transport for the properties of the air influencing the tropical cyclogenesis?

2. Model Setup and Observations

2.1. Numerical Model

The dust events between 9 and 14 September 2006 and the associated weather systems over West Africa were simulated using the Consortium for Small-Scale Modelling (COSMO) model (http://www.cosmo-model.org/) with the Aerosols and Reactive Trace gases (ART) module. COSMO is a nonhydrostatic limited area numerical model, based on the primitive equations that describe the compressible flow in a moist atmosphere [*Doms and Schättler*, 2002]. A generalized terrain-following height coordinate with rotated geographical coordinates and a grid stretching in the vertical are used for the coordinate system. The subgrid-scale moist convection is parametrized using the Tiedtke mass flux scheme [*Tiedtke*, 1989] with equilibrium closure based on moisture convergence. The subgrid-scale turbulence scheme is the 2.5 Mellor-Yamada closure [*Mellor and Yamada*, 1974]. Precipitation formation is treated by a Kessler-type bulk microphysics parametrization [*Kessler*, 1969] including water vapor, cloud water, cloud ice, snow, and rain with column equilibrium for the precipitating phase. The subgrid-scale clouds are parametrized by an empirical function of relative humidity and height. A δ-two-stream radiation scheme [*Ritter and Geleyn*, 1992] is used for the short- and long-wave fluxes and the full-cloud radiation feedback. The surface layer is parametrized by a stability-dependent drag law formulation of momentum, heat, and moisture fluxes according to similarity theory. A two-layer soil model [*Jacobsen and Heise*, 1982] employs the extended force-restore method.

The module ART describes the emission, transport, and deposition of gases and aerosols as well as their radiative feedback on the state of the atmosphere [*Vogel et al.*, 2009]. In the present study we will consider only mineral dust and not gases or other aerosols. Moreover, we concentrate on the interaction between dust and radiation. The mineral dust particles are represented by lognormal distributions. The dust emission scheme [*Vogel et al.*, 2006] combines the parametrization of the threshold friction velocity [*Lu and Shao*, 1999] and the saltation process [*Alfaro and Gomes*, 2001]. Mineral dust is emitted when the friction velocity exceeds a threshold friction velocity, which depends on the soil water content and surface roughness. The soil properties of 13 different sand types in *Chatenet et al.* [1996] are used. Details about the dust emission scheme, the radiation scheme, and the online calculation of the optical properties within COSMO-ART can be found in *Stanelle et al.* [2010]. Identical methods are used to calculate the transport of all scalars, i.e., temperature, humidity, and concentrations of gases and aerosols [*Vogel et al.*, 2009]. This includes the transport of scalars by deep convection which is parameterized with the Tiedtke scheme [*Tiedtke*, 1989]. The sedimentation and dry deposition of the mineral dust is treated according to *Binkowski and Shankar* [1995] and *Ackermann et al.* [1998]. The wet deposition of mineral dust is not included in the model set up for the present study. It is, however, a very important process that needs to be addressed in the future. Wet deposition depends strongly on the size of the dust particles, on the size distribution of falling hydrometeors, and on the intensity of the precipitation [e.g., *Mahowald et al.*, 2014]. Wet deposition removes the smallest and largest dust particles most efficiently. Far away from the source regions, where the large particles have usually already been deposited through dry deposition, the dust size spectrum is narrower and wet deposition dominates over dry deposition [e.g., *Bergametti et al.*, 1989; *Bergametti and Forêt*, 2014]. The exclusion of wet deposition may lead to an overestimation of mineral dust, particularly in the center of the storm and in MCSs. However, the exact effect of the wet deposition in different parts of the MCS and the developing tropical cyclone remains to be investigated.

The operational model setup includes a dust climatology where the desert aerosol dominates the continental aerosol. The desert aerosol optical thickness at 550 nm wavelength reaches values of up to 0.75 over the central Sahara and decreases toward high latitudes to values of 0.3 over central Europe [*Helmert et al.*, 2007]. This is appropriate for mean conditions, but for strong dust events the optical thickness is often underestimated [*Helmert et al.*, 2007; *Stanelle et al.*, 2010]. Thus, the dust climatology was switched off, and only the modeled dust concentrations are taken into account.

The initial and boundary conditions are taken from six-hourly European Centre for Medium Range Weather Forecasts (ECMWF) operational analysis which do not contain any information about dust concentrations and have a horizontal resolution of 0.25°. The COSMO-ART run has a horizontal resolution of 28 km and encloses

a domain from 0 to 45°N and −60 to 20°E. The coordinates are not rotated, and the model run is 144 h in duration. The model setup contains a hybrid system in the vertical which includes 50 levels with the top level at 20 hPa (about 28 km). The height of the sponge layer was increased from 11 km to 18 km, compared to the standard setup to allow for deep tropical convection.

This study is based on many COSMO-ART model runs, which compute the emission and transport of mineral dust aerosols, and the interaction between aerosols and radiation. A number of sensitivity studies were carried out to find the optimal model set up by, for instance, changing the start time, the domain size, the convective scheme, and conducting runs with no dust in the whole simulation, runs with dust as a tracer, and runs with the dust-radiation feedback switched on. In the following we will focus on the analysis of the model run with dust-radiation interaction that was initialized on 9 September 2006 at 12 UTC to diagnose the mineral dust pathways. The convection is parametrized, and the dust climatology is not applied so that only the modeled dust concentrations impact the radiation fields. The emission constant [*Vogel et al.*, 2006, Equation 3.7] is set to 0.8. The initial dust concentration is zero, which ensures that all the dust we will see in the following analysis originates over West Africa. The model initialization with no dust means that it takes some time before dust is emitted in the model run and that we can only analyze the model run after the dust is emitted and before the model run deviates too far from reality. The model spin-up time is roughly 6 h. The disadvantage of not including dust in the initial and boundary conditions is that the aerosol optical thickness in the model will always be lower than in reality as the dust advected from central, northern, and eastern Africa is not taken into account. Here we only consider the dust emitted over West Africa, which makes comparisons to satellite observations somewhat difficult.

This model setup is different to other studies, such as *Reale et al.* [2009] and *Sun et al.* [2009] where information on dust, temperature, and humidity is obtained via the assimilation of Atmospheric Infrared Sounder (AIRS) data. In contrast, COSMO-ART simulates the emission and the transport of mineral dust based on the current mineral dust distribution.

The emission of mineral dust during the model run is sufficient for the aim of this study, the procedure is more robust, and the results can be more easily interpreted than if the model is initiated with the limited data available. Observational data were used, however, to validate this run (see section 4).

2.2. Trajectory Calculations

Forward and backward trajectories, based on hourly model output, are used to diagnose the origin of the dust and the nature of its spatial evolution. The trajectories also help to illustrate the position of dry air relative to the tropical cyclone's center. The trajectories are calculated using the trajectory model LAGRANTO (Lagrangian analysis tool) [*Wernli and Davies*, 1997], with which the evolution of specific variables along the trajectories can be diagnosed. The trajectories start from every model grid point within a predefined three-dimensional domain.

2.3. Observational Data

West Africa and the Atlantic are data sparse regions. To validate the model results, we used observations which have different and, at times, incomplete spatial and temporal coverage due to the nature of the observations. We used all data available, which includes radiosondes over West Africa, flight measurements on board the DC-8 as part of NASA AMMA (NAMMA) campaign [*Jenkins et al.*, 2008], and a number of satellite products to give us the most complete overview of the region between 9 and 14 September 2006.

The horizontal distribution of dust is described using Meteosat Second Generation (MSG) Spinning Enhanced Visible and Infrared Imager (SEVIRI). Satellite images are produced from a combination of three infrared channels: 8.7, 10.7, and 12.0 μm. On these false color images [*Schepanski et al.*, 2007] the dust appears pink or magenta. These red-blue-green (RGB) dust images are useful to get an overview of where dust occurred during the period of interest and to qualitatively check the horizontal distribution of dust in the model run. They are, however, not well suited for a quantitative comparison.

Daily aerosol optical thickness (AOT) fields are obtained from the Moderate Resolution Imaging Spectroradiometer (MODIS)/Aqua Deep Blue Collection 051 over desertic surfaces (MOD08 product) and from MODIS/Terra over the ocean.

Information about the vertical distribution of dust over West Africa and the Atlantic is provided from the attenuated backscatter profile, or reflectivity profiles, at 532 nm retrieved from the spaceborne Cloud-Aerosol Lidar

with Orthogonal Polarization (CALIOP) on board the CALIPSO (Cloud-Aerosol Lidar and Infrared Pathfinder Satellite Observation) [*Winker and Hunt*, 2007] satellite with vertical and horizontal resolutions of 60 m and 12 km, respectively. The lidar-derived atmospheric reflectivity at 532 nm is mostly sensitive to aerosols with radii ranging from 0.1 to 5 μm, i.e., dust aerosols [*Flamant et al.*, 2007]. Between 9 and 14 September 2006 30 CALIPSO overpasses were available, but only a small number of them went through regions of interest. To validate the modeled dust concentration, we used three CALIPSO transects that went through the regions of high dust concentration in the model: transect 1 on 11 September 2006 from 1455 UTC to 1509 UTC, transect 2 on 12 September 2006 from 0306 UTC to 0320 UTC, and transect 3 on 12 September 2006 from 1359 UTC to 1313 UTC. More comparisons can be found in *Schwendike* [2010].

The SAL imagery from the Cooperative Institute for Meteorological Satellite Studies (CIMSS) highlights the presence of dry and/or dusty air between about 600 and 850 hPa [*Dunion and Velden*, 2004]. Both dry air and mineral dust lead to a positive "SAL" signal in these images. The total precipitable water (TPW) images were also provided by CIMSS. In the North Atlantic, 90–95% of the moisture is located below 500 hPa [*Dunion*, 2011]. Therefore, TPW provides an excellent representation of the low to middle level (about 600–925 hPa) integrated moisture in the column.

Additionally, we use radiosonde observations from the AMMA field campaign. The stations used are Dakar (17.49°W, 14.75°N) in Senegal, Tombouctou (4.1°W, 21.85°N) in Mali, and Nouakchott (15.95°W, 18.10°N) in Mauritania.

3. Dust Emission and Transport

In this section we will be looking quantitatively at the origins of dust laden as well as dry air over West Africa and how this air mass is transported toward the developing tropical cyclone Helene in the period between 9 and 14 September 2006.

3.1. The Main Weather Systems

A schematic shows the main weather systems over West Africa and the eastern Atlantic during the period of interest (Figure 1). On 9 September, an AEW is located over West Africa at 700 hPa, and embedded in the trough of this AEW is an MCS (Figures 1a and 1b). Details of this MCS can be found in *Schwendike and Jones* [2010]. As the MCS strengthens, it develops a gust front that also emits mineral dust (not shown). During the next days this AEW and the MCS move across West Africa and the eastern Atlantic. Over the Atlantic the convective system was classified a tropical depression on 12 September at 12 UTC. It intensified further and developed into Tropical Storm Helene on 14 September at 00 UTC and was upgraded to hurricane intensity on 16 September at 12 UTC. On 9 September (Figure 1a) at low levels, there was a monsoon trough located off the West African coast, and the south-southwesterly monsoon flow reached far across the West African continent. Strong northeasterly trade winds occurred along the West African coast west and east of the Atlas Mountains. Over West Africa they are referred to as the Harmattan. A subtropical anticyclone is located at low and middle levels of the northwest coast of West Africa. Note that the dimension of the anticyclonic circulation in the schematic is not intended to reflect the true size of the subtropical anticyclones in this region. Mineral dust is emitted north-northwest of the developing MCS (Figures 1a and 1b) and transported southwestward. There is also a band of dust along the northwest West African coast and in the lee of the Atlas mountains both in the observations and the model results.

At 700 hPa the AEW and the subtropical anticyclone move westward. Their approximate position on 11 September is shown in Figure 1c. At low levels the monsoon circulation is now much broader and overlaps with the AEW trough. Up to this day large amounts of mineral dust were transported upward over West Africa, as we will show in more detail later, and transported north of the AEW with the AEJ embedded within a large SAL outbreak that has emerged into the North Atlantic. However, part of the mineral dust is transported upward into the trough of the AEW and remains here as the AEW propagates westward. The northeasterly trade winds over the eastern Atlantic and over northern West Africa persisted. As the MCS moves westward, dust is transported across the Atlantic (Figure 1d). On 11 September at 2345 UTC (Figure 1f) dust is found north-northwest of the MCS and in a southwest-northeast orientated band north of the developing tropical storm. New regions with large amounts of mineral dust are present in the northeast of West Africa (Figure 1e).

When the low-level circulation and the circulation at 700 hPa were vertically aligned, the development of the pre-Helene tropical depression was initiated. The developing tropical storm is indicated by the hurricane

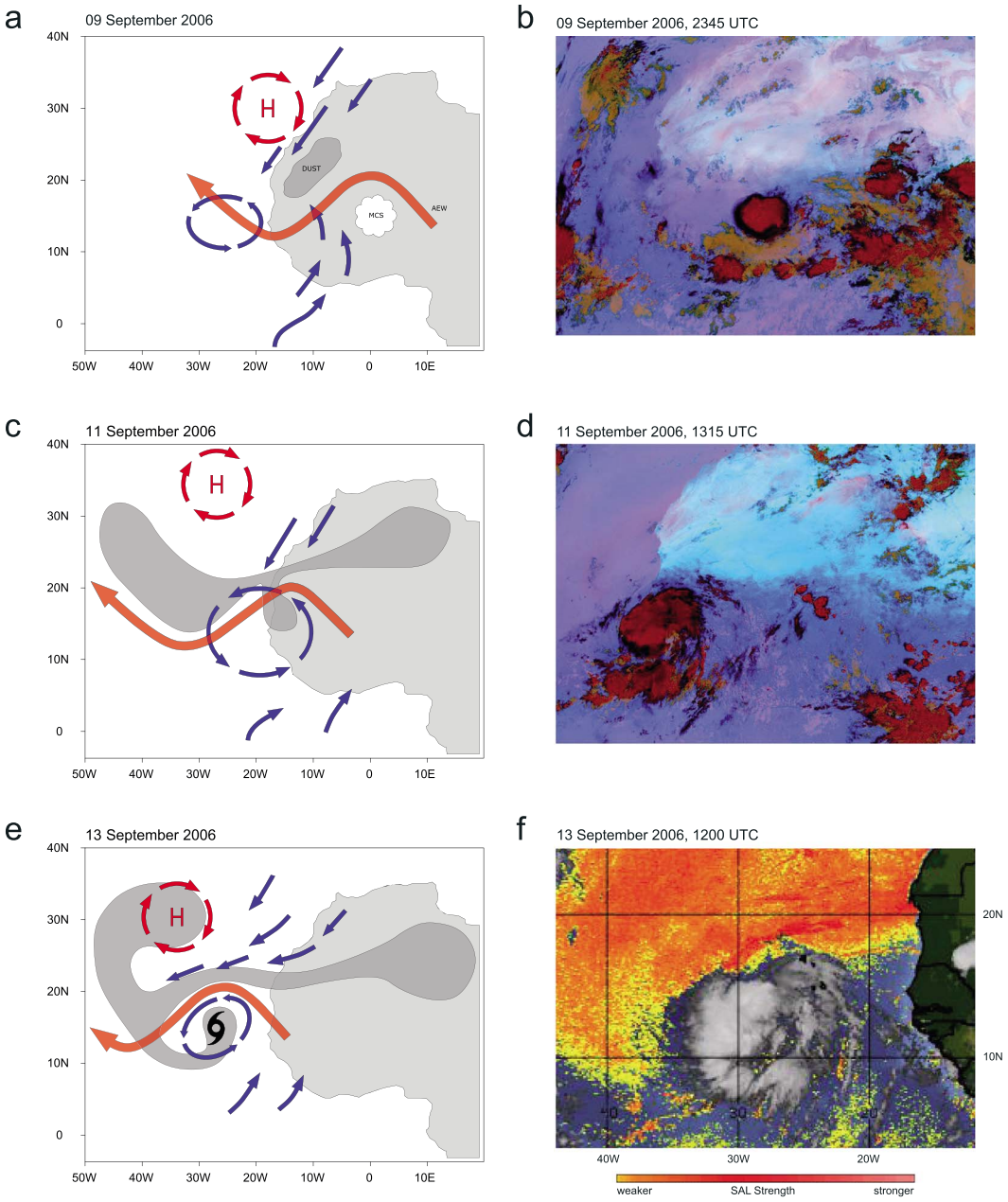

Figure 1. (a, c, and e) Schematic of the weather systems over West Africa and the eastern Atlantic and their approximate position during 9–13 September 2006. The red arrows illustrate the flow at 700 hPa, and the blue arrows the flow at 950 hPa. The mineral dust is displayed in a dark shade of grey. (b, d) The SEVIRI (Spinning Enhanced Visible and Infrared Imager) RGB dust product. Shades of pink illustrate dust in the atmosphere, and convection is displayed in colors of yellow and red. (f) The yellow to dark red colors illustrate weak to very dry and dusty air between about 600 and 850 hPa based on the difference between the 12.0 and 10.8 μm infrared channels on the Meteosat-8 satellite. Image courtesy of Jason Dunion ((Hurricane Research Division) HRD/CIMSS).

symbol in Figure 1e. There are distinct amounts of mineral dust in or near the center of the developing tropical storm (in the model run, Figure 1e) and northwest and north of it (Figure 1f). During the whole period there is a band of mineral dust located across Cap Blanc, which is a peninsula partly belonging to Mauritania and Western Sahara (see Figure 2 for its location).

Although the dust event between 9 and 14 September 2006 is of moderate intensity compared to other dust events that occurred in, for instance, March, June, and July of 2006, during which the AOTs reached values in the order of 3 [e.g., *Slingo et al.*, 2006; *Stanelle et al.*, 2010; *Bou Karam et al.*, 2009a, 2009b; *Flamant et al.*, 2009;

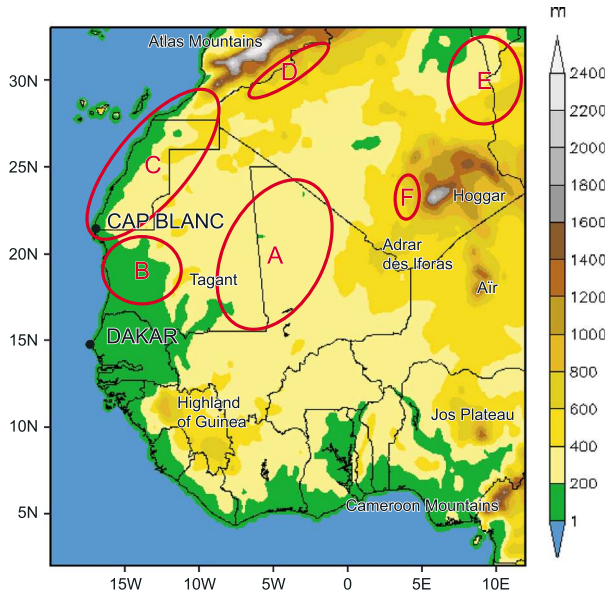

Figure 2. Political boundaries of the West African countries, the COSMO-ART model orography (meters above mean sea level) with a horizontal resolution of 28 km and the main source regions of mineral dust (A–F) in the period between 9 and 14 September 2006.

Kocha et al., 2012], the amounts of mineral dust were still relatively high. As we will see later, the AOTs for this case reached only up to 1.0, but these values are much more common over West Africa. We will also see later that during the whole tropical cyclogenesis of Hurricane Helene, mineral dust was present northwest and north of the developing system.

The period between 9 and 14 September was simulated with the model system COSMO-ART. The main source regions for the emission of mineral dust in the model run are shown in Figure 2. In region A, mineral dust was emitted due to increased northeasterly trade winds or a strong southwesterly monsoon flow. Dust was also emitted by the gust fronts of the convective systems over land (not shown) and due to orographical effects at the Atlas Mountains (region D), the branches of the Atlas Mountains in the Western Sahara (region C), and north and west of the Hoggar (regions E and F). Additionally, dust was emitted in association with the Atlantic inflow [*Grams et al.*, 2010] in region B. These source regions are in accordance with source regions found in SEVIRI satellite imagery (not shown).

3.2. Dust Emission and Low-Level Transport

The initial emission of mineral dust in the COSMO-ART model run initialized on 9 September at 12 UTC results from a cyclonic vortex embedded in the ITD and a low-level convergence line in the area between 15–26°N and 12–0°W on 9 September 2009 (region A in Figure 2). This frontal structure develops in a region characterized by a sharp temperature and humidity gradient and high values of positive relative vorticity (not shown). Strong Harmattan winds from the northeast reach down to about 18°N (Figure 3a) and cause the emission of significant amounts of dust in the Western Sahara (region C in Figure 2). Meanwhile, the moist monsoon flow reaches far north and turns to the northwest, west of the Greenwich meridian. Dust is emitted due to increased surface winds. This feature is restricted to the lower levels.

The region with maximum dust concentrations moves west-southwestward (Figure 3b). When the mineral dust reaches the West African coast line it is partly transported upward in the baroclinic zone along the coast, as we will see later in more detail. Due to the strong Harmattan and northeasterly trade winds near the northwest African coast, large amounts of dust are emitted and transported in the Western Sahara (Figure 3c). As seen in Figure 1, the largest amount of mineral dust occurs north-northwest of a mesoscale convective system over West Africa. Dust is also emitted by the convective system's cold pool, as can be seen when looking at all the SEVIRI RGB imagery for the period analyzed here. This is not represented by the model as the horizontal resolution of 28 km was too coarse to resolve the convective processes.

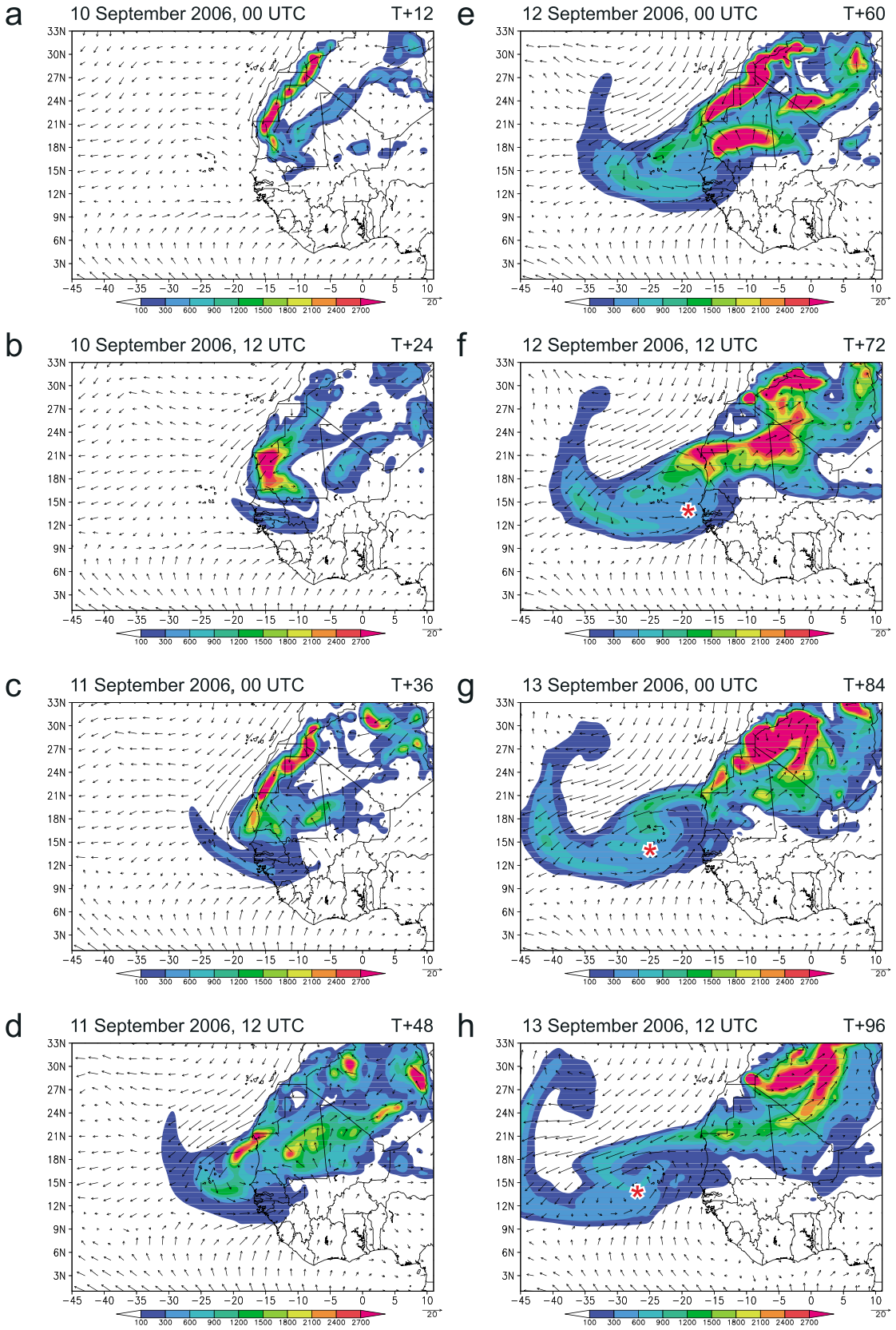

Figure 3. COSMO-ART simulation of mineral dust mass concentration (shaded, μg m^{-3}) and horizontal wind speed (arrows, m s^{-1}) at 950 hPa. The model run was initialized on 9 September 2006, 12 UTC. Asterisk gives approximate position of tropical depression in model simulation.

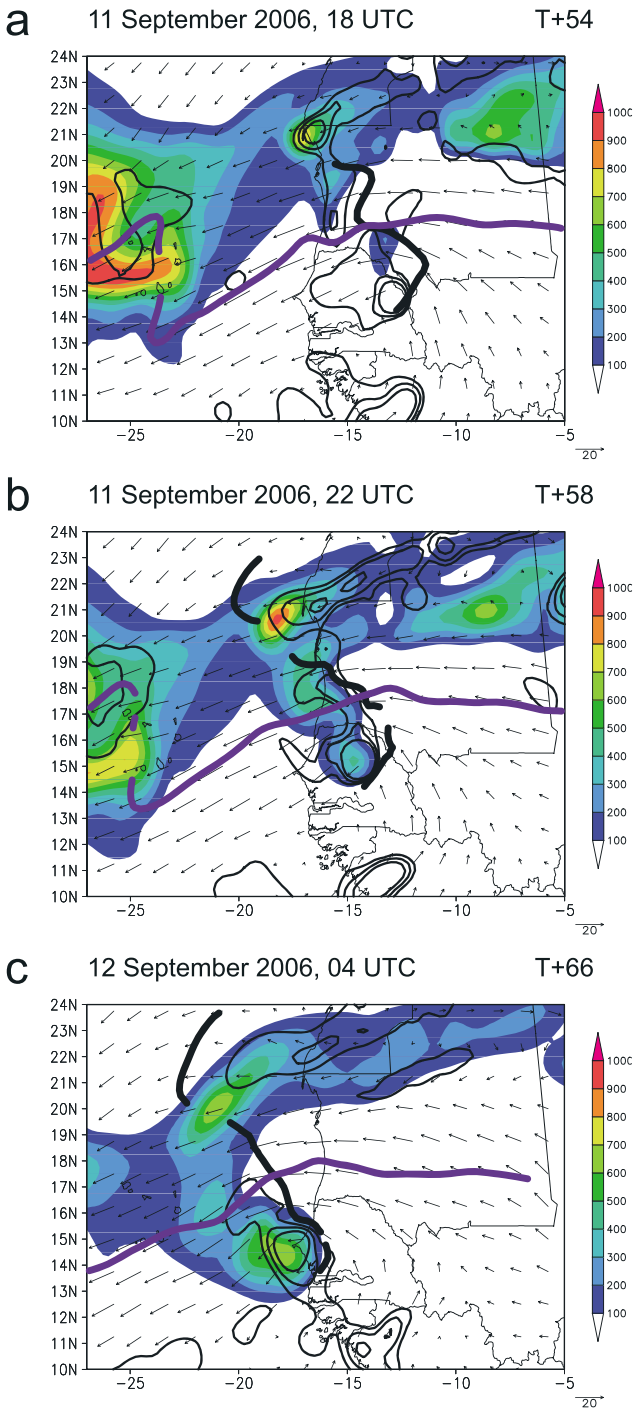

Figure 4. COSMO-ART simulation of mineral dust mass concentration (shaded, μg m^{-3}), horizontal wind speed (arrows, m s^{-1}), and ascent regions (−1.2 Pa s^{-1}, −0.6 Pa s^{-1}, and −0.2 Pa s^{-1} contours) at 700 hPa. The AEJ (purple) and AEW trough (black) axes were computed using the objective technique by *Berry et al.* [2007]. The model run was initialized on 9 September 2006, 12 UTC.

As the monsoon circulation, located partly over the eastern Atlantic and partly over West Africa, strengthens and moves further west, dust is transported not only westward but also cyclonically in the monsoon circulation over the ocean (Figure 3d). This way, some mineral dust reaches the West African coastline again south of Dakar and is transported upward when it reaches the coastal baroclinic zone, as we will be shown in sections 3.3 and 5. Other maxima in mineral dust mass concentration are located in the lee of the Atlas mountains and west and north of the Hoggar. Additionally, a new dust maximum occurs at around 18°N and 11°W due to the strong monsoon flow in that area. A few hours later, another major dust outbreak occurs in almost the same location (around 17°N and 11°W, not shown; see Figure 4a for mass concentration and regions of ascent for this event).

The emission of dust and its transport northward intensify in the following hours. This dust event is distinct in Figure 3e (18–21°N and 7–15°W). Part of that dust is transported upward shortly after the emission, part of the mineral dust is transported upward when it reaches the baroclinic zone along the West African coast, and a large part of the mineral dust is transported north-northwestward by the monsoon flow. High dust concentrations can also be see in the Western Sahara and the lee of the Atlas Mountains due to the strong Harmattan. In the region where the Harmattan and the monsoon flow converge the dust laden air is transported upward (Figures 3e and 3f). Part of the dust is transported further westward at lower levels and across the Atlantic. The dust remains in the monsoon flow as this circulation moved westward. Note that mineral dust occurs in and near the center of the developing tropical depression (Figure 3g).

High mass concentration can be seen in northern West Africa; part of the dust is transported by the low-level flow southwestward, parts are transported upward near Cap Blanc, and parts are transported northeastward. There is a continuous band of higher mass concentration around Cap Blanc. Shortly before the system reached tropical storm strength, mineral dust occurred nearly everywhere in the circulation at 950 hPa, and the highest concentrations were found in and north of the center of the circulation (Figure 3h).

3.3. Vertical Transport

In the afternoon hours on 11 September 2006 a significant dust event occurred in Mauritania (around 17°N and 11°W) leading to the high dust concentration in Figure 3e due to the enhanced monsoon flow that reached far north. In the early evening hours on 11 September mineral dust is transported upward at about 16–18°N and 12–14°W (Figure 4a). Relatively weak dust concentration can be seen at 700 hPa in this region. Higher dust concentrations occur along the West African coastline north of 19°N due to vertical transport of dust in the baroclinic zone here. A region with high dust concentration is located northwest of the AEW trough and is associated with dust that was advected by the AEJ from a previous dust event (Figure 3b). During the next four hours more dust is transported upward into the AEW trough (Figure 4b). The dust concentrations are particularly high west of Cap Blanc as the dust concentration near the surface in this area are high and thus more dust can be transported upward in the baroclinic zone along the coast. On 12 September at 00 UTC (Figure 3e), there is considerable low-level convergence and hence ascent at 950 hPa between about 14 and 20°N along the West African coast.

During the following hours, dust is transported upward along the coastal baroclinic zone into the AEW trough, where mineral dust concentrations in the order of 600–700 $\mu g\ m^{-3}$ can be found (Figure 4c). The high dust concentrations in the band across Cap Blanc occur in this area because the dust that is advected southwestward by the Harmattan and the dust that is advected northwestward by the monsoon flow are transported upward at the convergence line between Harmattan and monsoon, the ITD.

As the AEW propagates westward, the dust in the AEW trough is also transported westward. Until the afternoon of 11 September, dust occurred north and northwest of the AEJ and was transported upward at the ITD and at the baroclinic zone along the coastline north of the AEW and transported westward by the AEJ. Due to the dust event in the late afternoon hours on 11 September and the fact that the dust was transported upward mainly in the costal baroclinic zone and by convection in the AEW trough, it reached heights of about 700 hPa in the AEW trough. It shows that during the early development stages, mineral dust was present in the vicinity and in the center of the tropical depression. This southern dust event cannot be seen in the satellite images but could have been masked by the large cirrus shield of the convective system over the Atlantic on 11 September 2006 (Figure 1d).

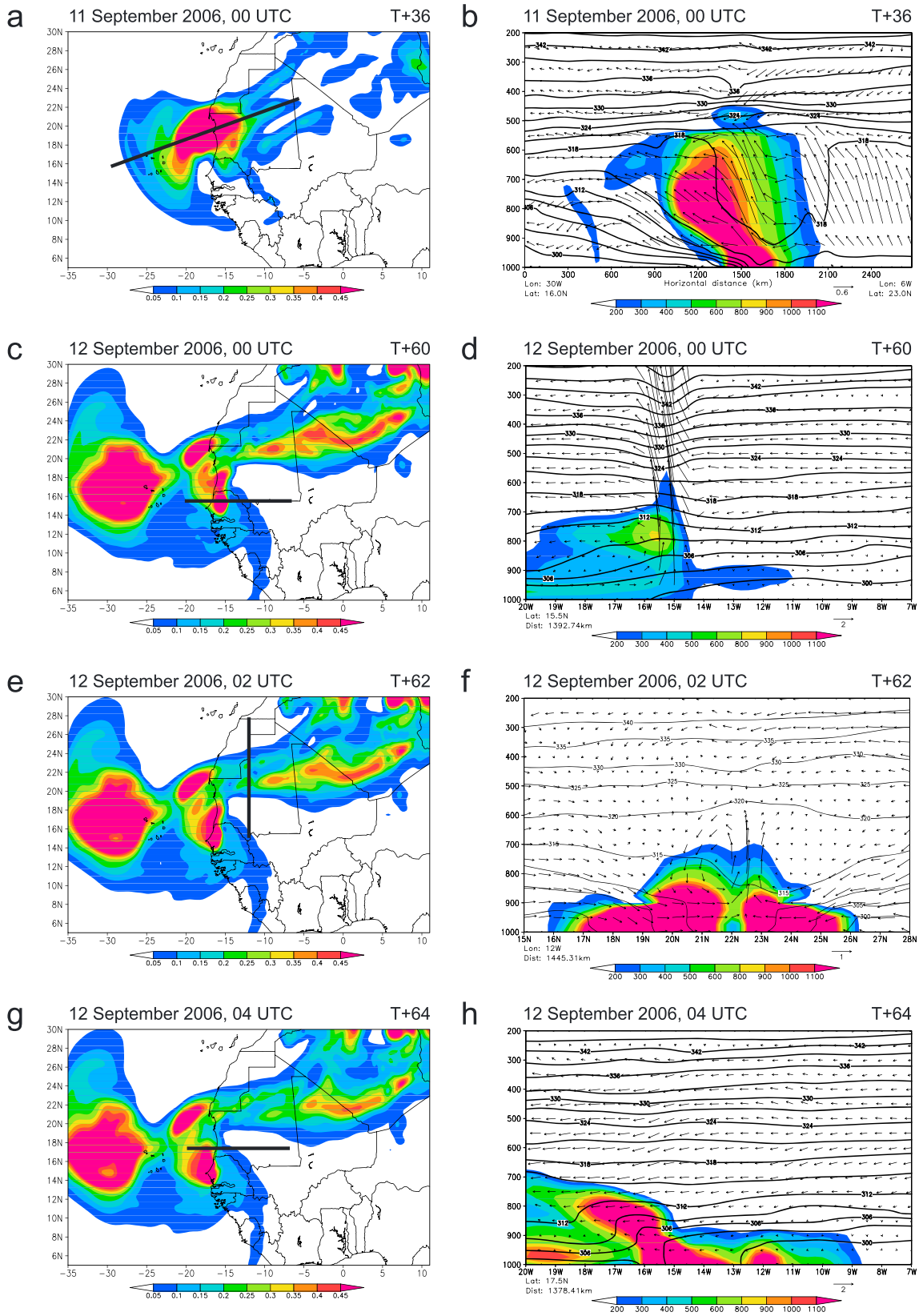

Figure 5. (a, c, e, and g) The aerosol optical thickness (shaded). The black solid line displays the position of the cross section on the right. (b, d, f, and h) The mineral dust mass concentration in μg m^{-3}, the potential temperature (K) in contours, and the wind in the plane of the cross section. Pressure in the vertical component. The model run was initialized on 9 September 2006, 12 UTC.

Mineral dust is transported upward mainly in the baroclinic zone along the ITD, the baroclinic zone along the West African coastline, and by convection. These processes are illustrated in the following by selected cross sections (Figure 5).

A cross section through the region of largest AOT on 11 September at 00 UTC (Figures 5a and 5b) shows that the dust is lifted upward along the isentropes in the region with the strongest potential temperature gradient due to the warm air of the Saharan heat low to the northeast and the colder air of the maritime region in the southwest. Isentropic upgliding [*Bou Karam et al.*, 2008] in the baroclinic zone between the maritime and the Saharan air is indicated at 1300–1600 km (Figure 5b). The isentropic upgliding occurs in the baroclinic zone along the coast and transports mineral dust up to a height of about 500 hPa; it then descends slightly. At 700 hPa, significant amounts of dust are transported across the Atlantic.

Mineral dust is also transported upward by convection, which includes dry convection and nonprecipitating convection over West Africa and moist convection over the Atlantic. This is one mechanism for dust transport into the AEW trough. However, with a resolution of 28 km this model run does not represent convection accurately as convection is parametrized. The mass concentration of this mineral dust event is relatively small compared to other dust events in the period analyzed here. The cross section on 12 September at 00 UTC shows distinct vertical ascent between 16 and 14°W which transports mineral dust from lower levels upward (Figures 5c and 5d). This process started a few hours before which is why the dust maximum occurs between 700 and 800 hPa. The cross section shows also that part of the low-level inflow into the convective system exits at around 800 hPa and above. This behavior has been observed previously in a high-resolution model simulation of an MCS over West Africa by *Schwendike and Jones* [2010]. Convective cells that were embedded in an MCS (Figure 1d) are likely responsible for the high vertical velocity in that region and thus the vertical transport of dust.

The region of high AOTs over the Atlantic (Figures 5c, 5e, and 5g) results from the mineral dust that was emitted by the trade wind flow, transported southwestward by the Harmattan, when it reached the coastal baroclinic zone transported upward (Figures 5a and 5b) and was then transported westward by the AEJ.

The mechanisms for vertical transport of mineral dust along the ITD have been described in detail by *Bou Karam et al.* [2008]. The vertical transport of dust for this case study is illustrated in Figures 5e and 5f. On 12 September at 2 UTC, it is apparent that the monsoon flow from the south and the Harmattan from the north approach each other and advect significant amounts of dust. Both flows converge between 22 and 23°N. In this region the dust laden air is transported upward. When the dust reaches the height of the AEJ, it is transported westward.

To illustrate how the dust gets into the AEW trough, we chose a cross section on 12 September at 4 UTC (Figures 5g and 5h). At the time the monsoon trough was the dominant feature at the West African coast and the low-level flow mainly came from the southeast. Hence, the coastal baroclinic zone was much weaker than the one in Figure 5b. Here the center of the monsoon trough is offshore, and the wind in the western part of the cross section is relatively weak. This region contains already mineral dust that has been advected here previously by the monsoon trough circulation. The dust is transported upward in the albeit weak baroclinic zone along the West African coast into the trough of the AEW. The dust reaches up to 700 hPa, and the dust laden air is distinctly warmer than the environment.

The diurnal cycle of the coastal baroclinic zone alters the vertical transport of dust [e.g., *Parker et al.*, 2005b]. The baroclinic zone, roughly between Cap Blanc and Dakar, develops in the afternoon hours and reaches maximum strength at around 18 UTC, when the temperature contrast between the cool maritime air and the hot Saharan air is strongest (not shown). Then the baroclinic zone moves inland and decays in the early morning hours (around 3 UTC). That means that the temperature gradient is weak or nonexistent where the maritime flow crosses the coast. Often, this inland movement is associated with the emission and transport of mineral dust. This is very similar to the behavior of the Atlantic inflow described by *Grams et al.* [2010]. This behavior is, however, altered by the position of the monsoon trough. The coastal baroclinic zone was weakened when the center of the monsoon trough was located just offshore the West African coast.

The Okubo-Weiss (OW) criterion, which designates flow regimes dominated by rotation, can be used to distinguish regions of parcel accumulation and parcel dispersion, for instance, highlight regions where mineral dust is trapped. We calculated the OW criterion following *Hua and Klein* [1998]: $OW = E^2 - \zeta^2$,

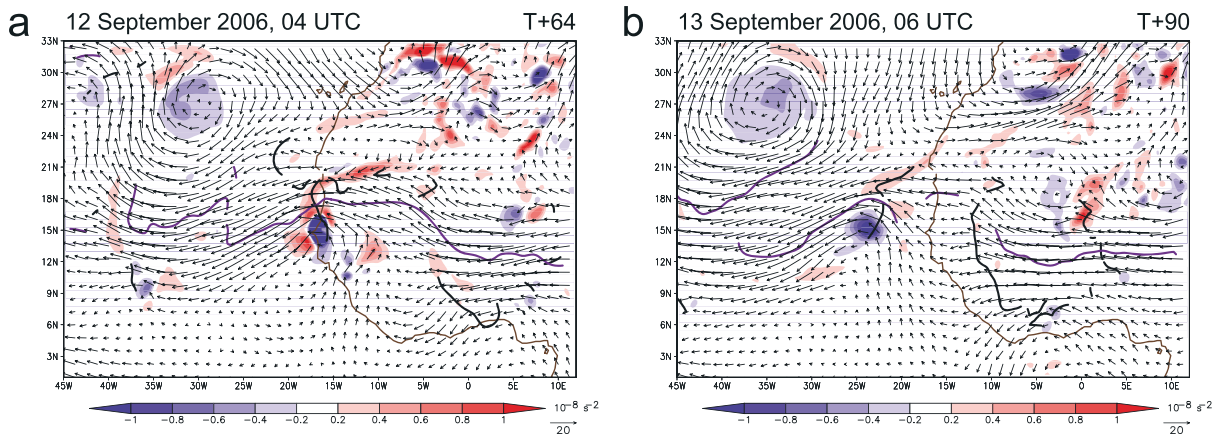

Figure 6. The Okubov-Weiss criterion (s^{-2}), the horizontal wind speed (arrows, m s^{-1}), and the jet (purple) and trough (black) axes computed using the objective technique by *Berry et al.* [2007]. The model run was initialized on 9 September 2006, 12 UTC.

where $\zeta = \partial v/\partial x - \partial u/\partial y$ is the vertical component of the relative vorticity and E is the rate of strain with $E^2 = E_{sh}^2 + E_{st}^2$. The shearing deformation is given as $E_{sh} = \partial v/\partial x + \partial u/\partial y$, and the stretching deformation is $E_{st} = \partial u/\partial x - \partial v/\partial y$.

In those regions where the OW criterion is negative, i. e., where the flow is strongly curved and dominated by rotation, parcels are trapped. This means that dust particles that reach the AEW trough remain there. From very early on in the simulation, parcels in the AEW trough are trapped as the OW criterion has small negative values in that area. As convection develops in the AEW trough the negative OW criterion becomes more confined and intensifies. On 12 September at 4 UTC, when dust is transported upward into the AEW trough and a MCS occurs in the coastal region south of Dakar, the dust laden air is confined in the AEW trough (Figure 6a). North and west of this region of strong negative OW criterion, the criterion changes sign. As the AEW moves further west and the tropical depression develops, the OW criterion is strongly negative in the AEW trough (Figure 6b). This is consistent at all levels.

This model simulation shows that the mineral dust is transported in different ways. During the whole period, mineral dust is emitted and transported upward north of the AEJ axis. Once it reached the AEJ it is transported westward by the AEW. This leads to distinct mineral dust concentrations north and northwest of the tropical storm. We also showed that dust is transported upward by convection and in the baroclinic zone along the West African coastline into the AEW trough. Once the dust reaches this position it stays in the trough and is transported with it.

4. Comparison Between Observations and Model Results

To validate the model results, we mainly used satellite data as West Africa and the eastern Atlantic are data sparse regions with respect to in situ data. Additional comparisons with satellite data and radiosoundings from the AMMA campaign can be found in *Schwendike* [2010]. Note that the satellite products do not provide a complete spatial and temporal coverage.

The horizontal AOT distribution in the model is similar to the MODIS AOT distribution in the Terra satellite imagery (Figure 7). High AOTs occur just off shore the West African coastline roughly between Dakar and Cap Blanc on 10 September 2006, as can be seen in both the model run and the observations (Figures 7a and 7b). On 12 September, the position of a north-south oriented band of dust ahead of the AEW out of which Hurricane Helene developed (12–30°N) is depicted by the model (Figures 7c and 7d). The band of mineral dust across Cap Blanc (between 19 and 23°N) is distinct in the model run as well as in the satellite imagery. The high AOT values seen in the model run at around 12–15°N and 18–23°W are masked by clouds in the satellite product and cannot be verified. The model results also show that the highest AOTs occur west and southwest of Cap Blanc as seen in the satellite images. Comparisons between the model results and the AOT from Modis deep blue on Aqua over land (not shown) revealed that the maxima of the dust concentration appear to occur in the right places, i.e., in the regions illustrated in Figure 2. The overall dust concentrations, however, seems to be too low in the northeastern and eastern part of the model domain. This is due to the fact

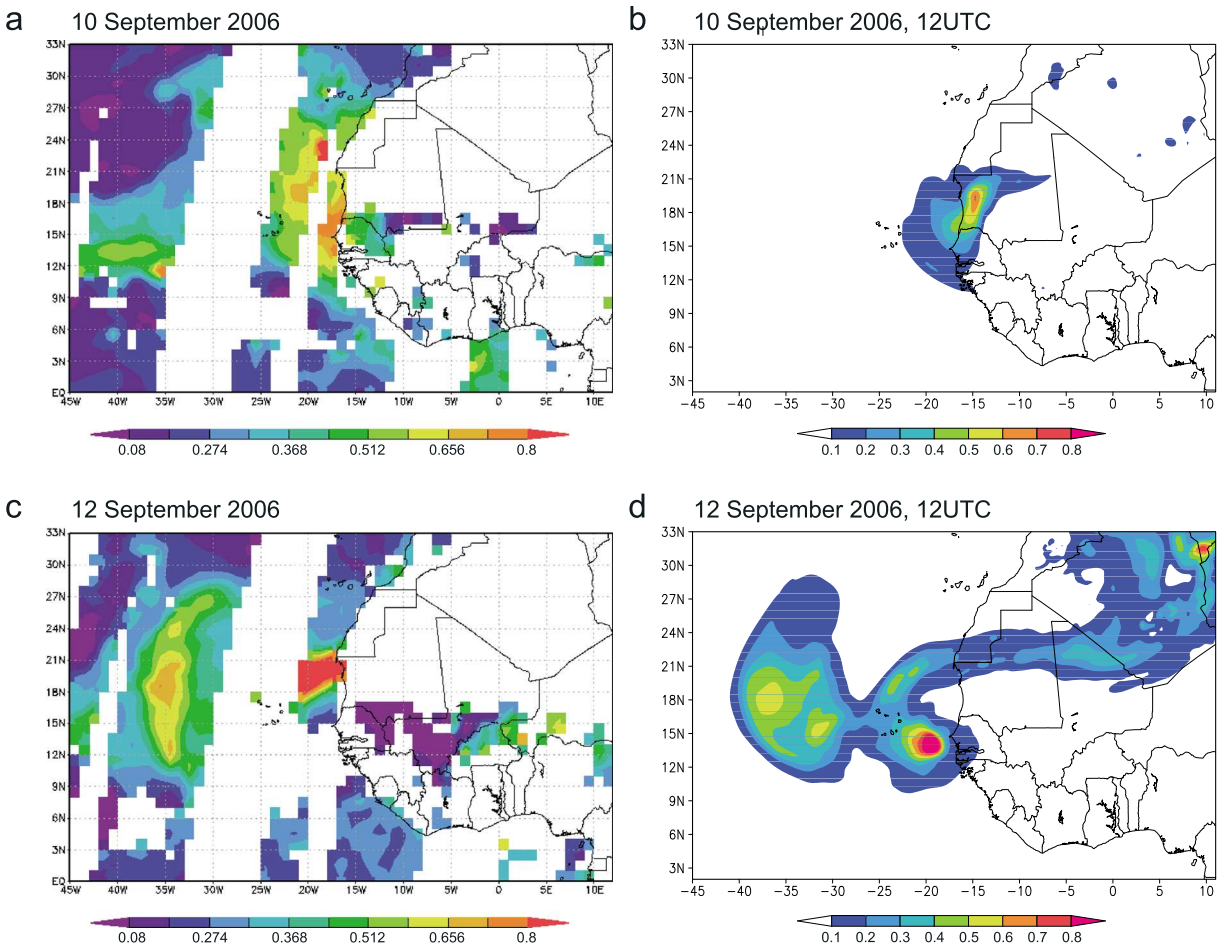

Figure 7. Aerosol optical thickness (AOT) from MODIS on Terra on (a) 10 September and (c) 12 September 2006. These visualizations were produced with the Giovanni online data system, developed and maintained by the NASA Goddard Earth Sciences Data and Information Services Center (GES DISC). The AOT on (b) 10 September and (d) 12 September 2006 at 12 UTC, based on the model run initialized on 9 September 2006, 12 UTC.

that the dust concentration is zero in the initial and boundary fields. Thus, no dust is advected into the model domain. Moreover, it is not possible to include all source regions into the model domain due to computational restriction.

A comparison of the COSMO-ART run with CALIPSO transects (Figure 8) shows that the vertical extent of the dust layer is well represented in the model. On 11 September 2006 at 15 UTC, the highest dust concentrations over the Atlantic occur at 600 hPa and in the levels below. The uplifted dust region is distinct in the model results as well as in the CALIPSO image (Figures 8b and 8c). The high concentrations near the surface toward the southern end of the cross section might be due to dry and wet deposition of mineral dust aerosols as this end is closer to the continent, i.e., the source region, and mainly due to the fact that mineral dust is advected southwestward over the eastern Atlantic by the monsoon trough. The maximum dust concentrations between the near surface and about 800 hPa are located in the southeastern end of the cross section, i.e., in the monsoon trough (Figures 3b and 3c).

High dust concentrations between 700 and 800 hPa can be seen in both the CALIPSO transect and the modeled cross section on 12 September at 03 UTC (Figures 8e and 8f). The high low-level concentrations in the northeastern part of the cross section are also apparent. They occur in the region around Cap Blanc, where dust concentrations in the order of 3000 $\mu g\ m^{-3}$ are transported over the Atlantic. Due to deep clouds at the southwestern end of the cross section, the southern low-level dust concentration cannot be validated using the CALIPSO image.

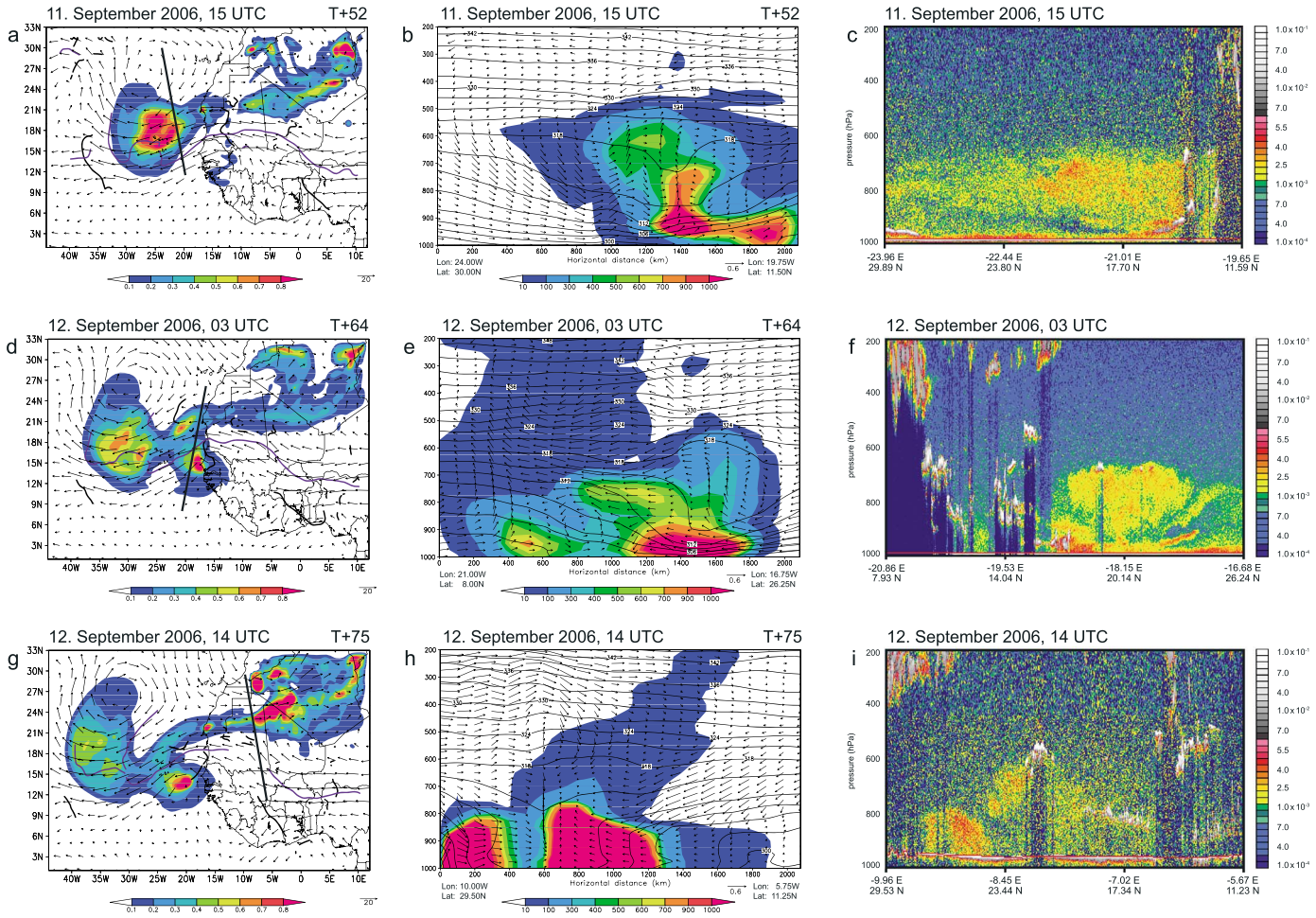

Figure 8. (a, d, and g) AOT (shaded) and the horizontal wind speed (m s^{-1}) from the COSMO run initialized on 9 September 2006, 12 UTC. The black and purple curvy lines denote the AEJ trough and jet axes computed after the method from *Berry et al.* [2007], respectively. The straight black lines show the position of the cross section. (b, e, and h) The mass concentration (μg m^{-3}, shaded), potential temperature (3 K contour interval), and wind speed (arrows in m s^{-1}) along the cross section shown in Figures 8a, 8d, and 8g. (c, f, and i) Vertical damped backscatter coefficient at 532 nm (km^{-1} sr^{-1}) from CALIPSO. Signal strength is color coded with blue making weak molecular scatter and very weak scattering on aerosols. Aerosols are shown in yellow, orange, and red. Strong cloud signals are given in grey and weak cloud signals in red and yellow. The validation time is given at the top of every figure, and the forecast time is shown in the top right corner in Figures 8a, 8b, 8d, 8e, 8g, and 8h. The pressure is the vertical coordinate for the cross section.

The model is able to simulate the high dust concentrations that occur on 12 September 2006 at 14 UTC over land (Figures 8h and 8i) due to strong northerly flow south of the Atlas Mountains and at the ITD and even the region of much lower concentration between 9 and 8°E. The uplifted dust that reaches altitudes of about 650 hPa is also simulated. The modeled maximum dust concentration over land (Figure 8h), owing to the convergence between the Harmattan and the monsoon flow along the ITD, is seen in the satellite image (Figure 8i). However, the southern maximum in the satellite image is covered by clouds. Dust is present even above 600 hPa, albeit with low concentrations. The northern maxima in dust concentration can be related to the Harmattan and the dust source region in the lee of the Atlas Mountains. In general, these comparisons show a reasonable agreement between model results and observations.

Lidar measurements of the aerosol concentration (Figure 9a) on board the NAMMA DC-8 on 12 September 2006 [*Jenkins et al.*, 2008] along the flight path shown in Figures 9c and 9d, display the same vertical extent of the dust layer as in the COSMO-ART run (Figure 9b). These measurements also show relatively high mineral dust concentrations near the surface at the northern end of the cross section. Additionally, this dust laden layer is characterized by relatively low specific humidity values in both the measurements and the model results (around 3–6 g kg^{-1}; not shown). This indicates that the relatively high dust concentrations in the COSMO-ART simulations at lower levels (Figure 9b) are not unrealistic.

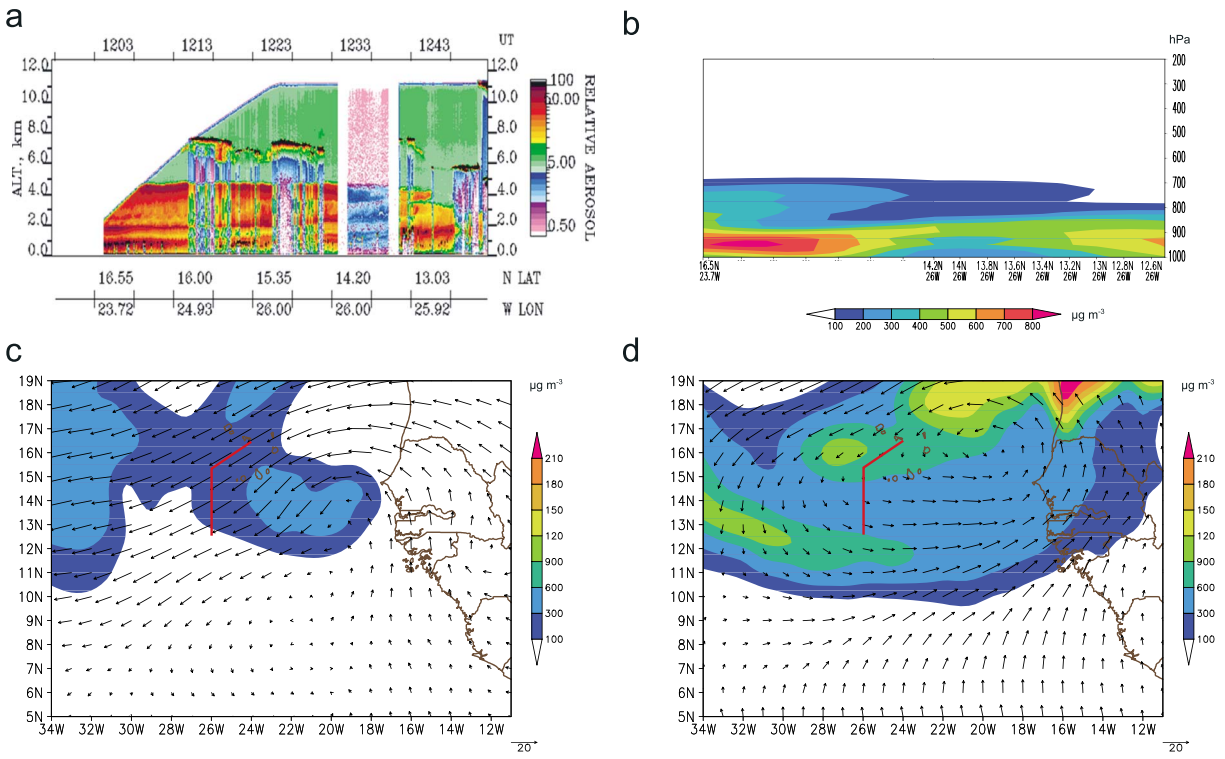

Figure 9. (a) NAMMA Lidar Atmospheric Sensing Experiment (LASE) imagery of aerosol scattering between 1200 and 1248 UTC on 12 September 2006. Taken from *Jenkins et al.* [2008], their Figure 3. (b) Mineral dust mass concentration (μg m^{-3}) along the same transect as in (a) at 12 UTC (T + 72) based on the model run initialized on 9 September 2006 at 12 UTC. (c, d) Mineral dust mass concentration (μg m^{-3}) and horizontal wind (m s^{-1}) at 700 hPa and at 975 hPa, respectively, on 12 September 2006 at 12 UTC (T + 72) based on the model run initialized on 9 September 2006 at 12 UTC.

We extend our analysis of the SAL by investigating the moisture distribution in more detail. We compared the vertical integral of cloud water, cloud ice, and water vapor, henceforth total water, with the total precipitable water (TPW) from satellite data (Figure 10). *Dunion* [2011] defined mean values of TPW based on a multiyear composite of tropical North Atlantic soundings. He found that 45 mm is a good threshold for identifying moist environments like the moist tropical sounding (55 mm) compared to dry environments like the SAL (40 mm) and middle altitude dry air intrusions (38 mm). The distribution of dry air in the TPW satellite images is remarkably similar to the total water images based on the COSMO-ART run even at forecast times of 120 h. On 12 September 2006 at 12 UTC the region with total precipitable water smaller than 35 mm north of Cap Blanc extends to about 18°N and 30°W in the both the satellite image and the model run (Figures 10a and 10b). The largest values in total water content can be found between about 12 and 18°N, 21 and 17°W in both images, but a region with even higher values in total water occurs southwest of it in the satellite image. During the next 24 h, the band of dry air extends southwestward, increasing the temperature gradient northwest of the tropical depression (Figures 10c and 10d). Particularly, dry air is present on 13 September 2006 at 12 UTC between Cap Blanc and about 30°W north of 22°N in the model data and north of 19°N in the satellite image. A second region of very dry air can be found between 15–22°N and 42–37°W. As the storm further intensifies, a band of high total water values in the southwest and northeast of the storm's center can be observed in the satellite and model data (Figures 10e and 10f). The convective system associated with the high total water has about the same position in both the simulation and the satellite images. Even after a forecast time of 120 h (Figures 10e and 10f), the position of the storm, the region of very dry air north of the tropical storm, and the band of moist air are in accordance in both images.

The mineral dust is very marked to the north and north west of the developing tropical depression between 12 September 2006 and 14 September 2006 (Figure 11). The potential temperature anomalies at 700 hPa (not shown) are largest north of the convective system and north of the AEW as well as in the ridge ahead of the AEW in which the pre-Helene system develops. This relatively warm air is also characterized by low values of specific humidity (0–6 g kg^{-1}) and high AOTs (Figures 11b, 11d, and 11f). The highest dust concentrations occur just north of the middle level circulation center on 12 September 2006 (Figure 11b).

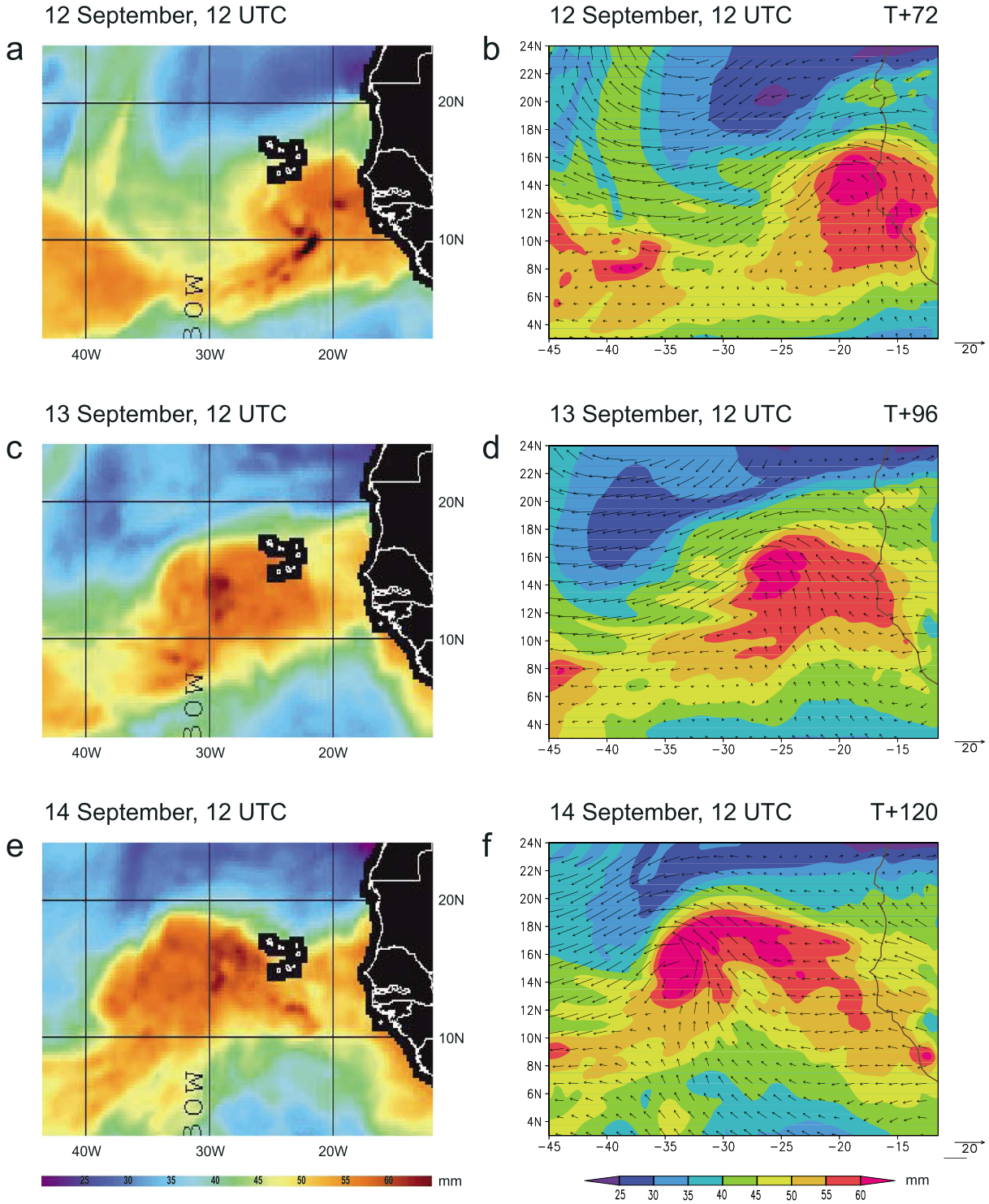

Figure 10. (a, c, e) Total precipitable water (TPW) in mm based on the sensors SSM/I on the DMSP 13/14 satellites and the Advanced Microwave Scanning Radiometer–EOS sensor on the Aqua satellite are used for the shown image. The black squares over the Cape Verde Islands occur because TPW is not estimated over ground. Image courtesy of Jason Dunion (HRD/CIMSS). (b, d, f) The vertical integral of cloud water, cloud ice, and humidity (mm), and the horizontal wind speed (m s^{-1}) at 700 hPa based on the COSMO-ART run initialized on 9 September 2006, 12 UTC.

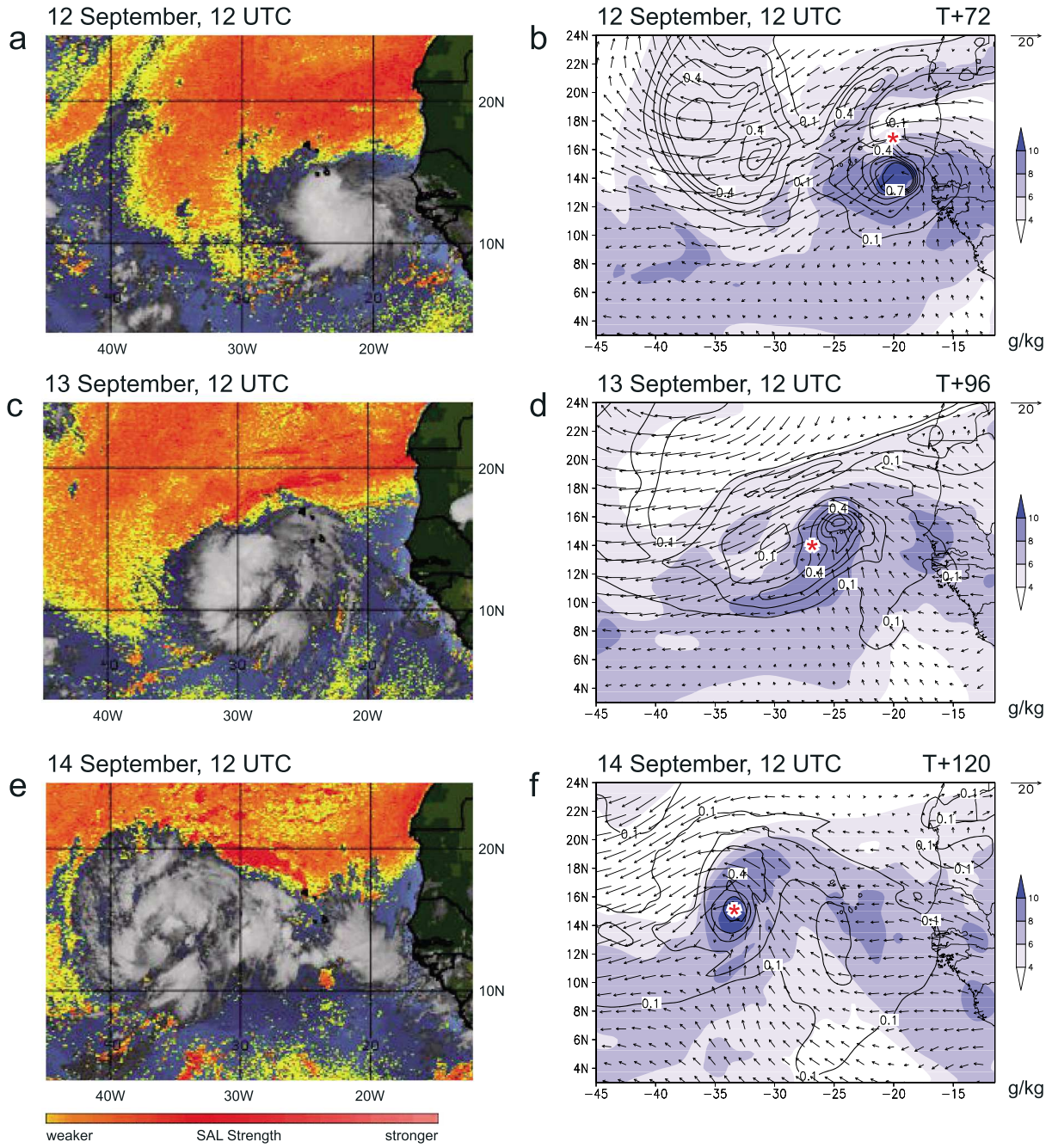

Figure 11. (a, c, e) The Saharan air layer (SAL) based on the difference between the 12.0 and 10.8 μm infrared channels on the Meteosat-8 satellite. The yellow to dark red colors illustrate weak to very dry and dusty air between about 600 and 850 hPa. Image courtesy of Jason Dunion (HRD/CIMSS). (b, d, f) Specific humidity (g kg^{-1}, shaded), aerosol optical thickness (contours), and horizontal wind speed (m s^{-1}, arrows) at 700 hPa based on the COSMO-ART run initialized on 9 September 2006, 12 UTC. The red star marks the position of the center of the low-level circulation.

Note that the band with relatively high specific humidity along about 20.5°N and between 18–10°W occurs in the convergence zone between the Harmattan and the monsoon flow, i.e., the ITD. This region is also characterized by positive relative vorticity and ascent (not shown), which leads to increased humidity at 700 hPa and the vertical transport of mineral dust.

The satellite imagery (Figures 11a, 11c, and 11e) shows the dry and dust enriched air surrounding the convective system, particularly in the north-northwest. We cannot assess whether the regions of dusty air were in fact

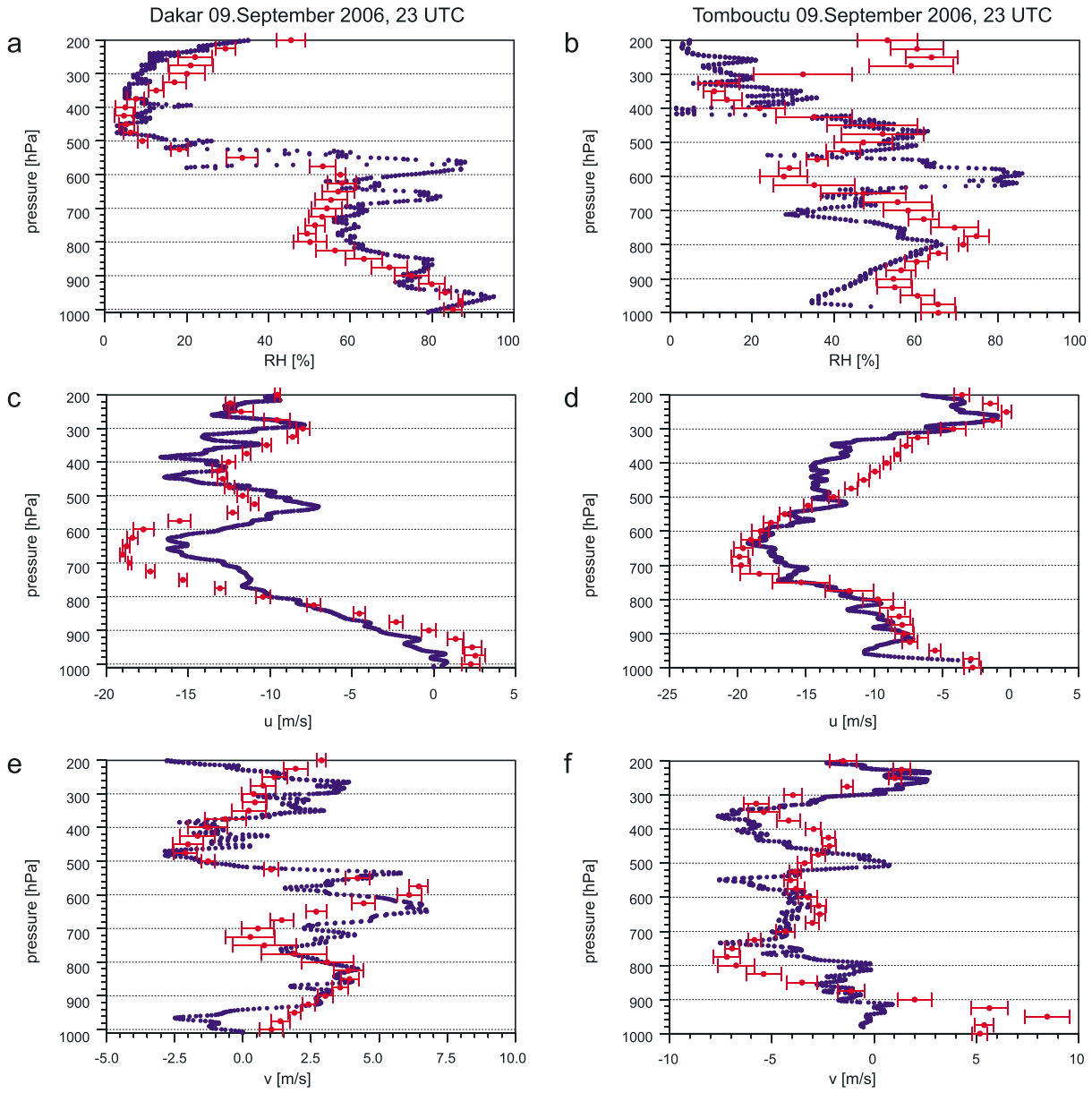

Figure 12. Profiles of (a, b) relative humidity (%), (c, d) the zonal wind (m s^{-1}), and the meridional wind from radiosondes, released in Dakar (17.49°W, 14.75°N), Senegal, at (a, c, e) 9 September 2006, 2235 UTC, and at (b, d, f) 2232 UTC on 9 September 2006 in Tombouctou (4.1°W, 21.85°N), Mali. The radiosounding is displayed by blue dots and the corresponding model output from the 144 h COSMO forecast initialized at 12 UTC on 9 September 2006 by red dots. The horizontal bars indicate the standard deviation of the model output in a 0.5° × 0.5° square centered on the closest grid point.

present but could not be detected in cloudy regions. However, we provide a dynamically valid explanation for its presence.

The pre-Helene convective system was classified a tropical depression on 12 September at 12 UTC. During the next 24 h, the system strengthened and the region of high AOTs elongated. The dry and warm air ahead of the tropical depression extends down to 10°N as does the dry and possibly dusty air indicated in the satellite imagery (Figures 11c and 11d). Relatively high dust concentrations are transported across the West African coast around Cap Blanc as seen in high AOTs in that region and in the dark red region in the corresponding satellite image. As the system develops, dry and, most likely, wet deposition takes place so that the AOTs decrease. The simulated AOT in the storm's center is still higher than in its environment. Bands of relatively dry and possibly dusty air spiral toward the storm's center in the south and east of the tropical storm on 14 September 2006 (Figures 11e and 11f). During the tropical cyclogenesis, dry air was always present to the west

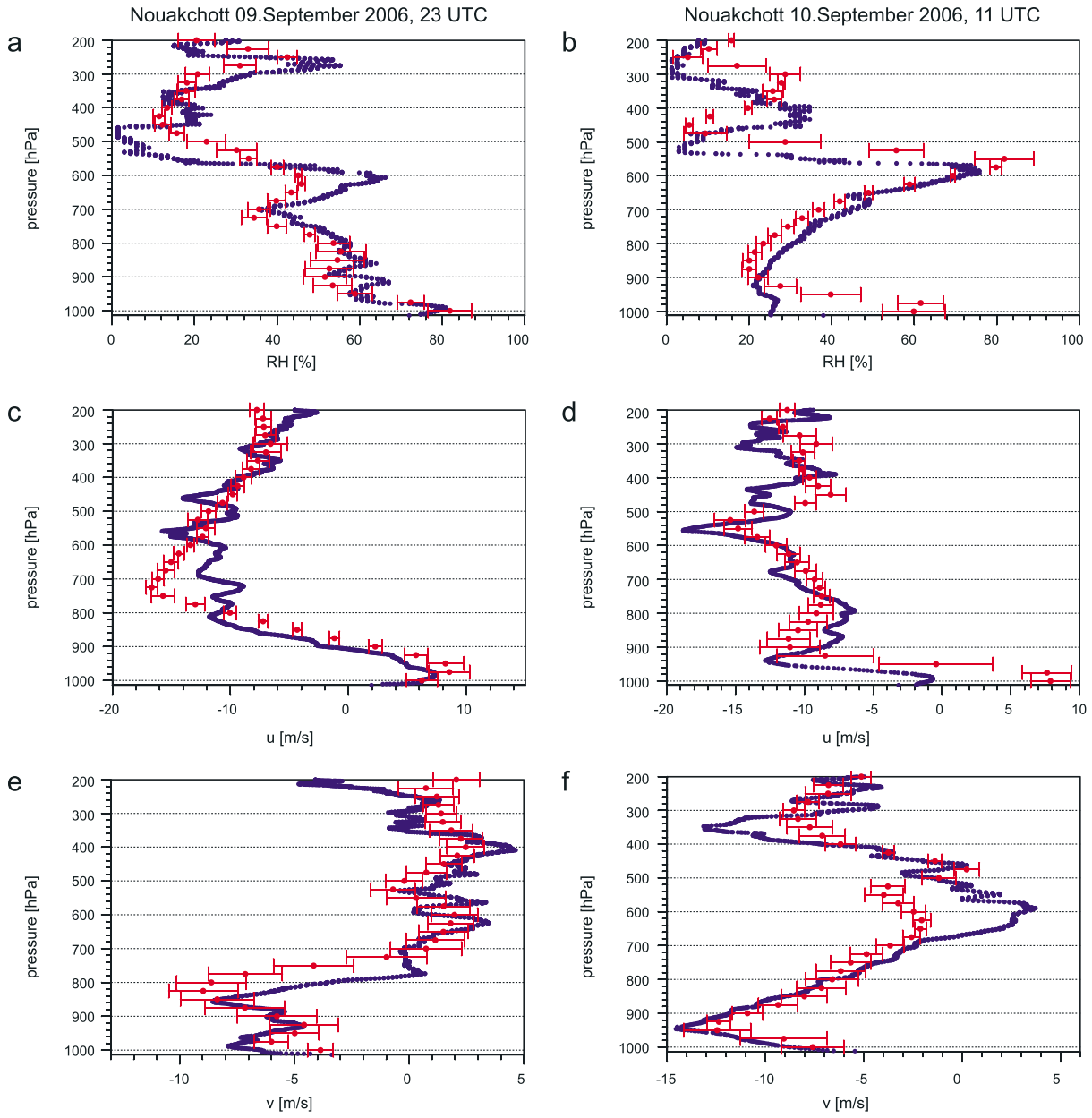

Figure 13. The same as Figure 12, but the radiosounding in Nouakchott (15.57°W, 18.6°N), Mauritania, on (a, c, and e) 9 September 2009, 2234 UTC, and on (b, d, and f) 10 September at 1042 UTC.

and north of the tropical depression, which is in accordance with the satellite images in Figure 11. Additionally, distinct amounts of mineral dust are located in the AEW trough and in the center of the tropical storm.

The orange-red color coded regions in the satellite images (Figures 11a, 11c, and 11e) highlight regions that are either dry, dust enriched, or both. The AOT distribution in the COSMO-ART run shows that the southern portion of the "SAL" closest to Helene is both dry and dusty implying the origin over West Africa, the westernmost portion of orange SAL is also dusty, the portion to the north and intruding southward (north of 18°N and between about 25 and 40°W, Figure 11d) is dry but dust-free air, and the region of the developing tropical storm is dust enriched and relatively moist.

The model representation of moisture and wind fields is validated using radiosoundings from the AMMA database. The soundings in Dakar and Tombouctou (Figure 12) illustrate the conditions before the dust events. The AEJ is located at about 650 hPa in both stations with values of around −20 m s^{-1} (Figures 12c and 12d).

Tombouctou is located north of the jet, and Dakar is located underneath the jet axis in the ridge of the proceeding AEW. The meridional wind is markedly smaller than the zonal wind, although a maximum occurs over Dakar with about 7 m s^{-1} at 650 hPa (Figure 12e) and of the opposite sign in the middle troposphere over Tombouctou. The moisture profiles of both stations (Figures 12a and 12b) differ significantly. The near-surface air layer is very moist (80–100% relative humidity) over Dakar due to the maritime influence. Between about 14 and 19°N westerly flow (Atlantic inflow) occurs along the West African coast line [*Grams et al.*, 2010]. Above this layer in the lower troposphere the relative humidity decreases with height but increases again at middle levels. In Tombouctou the lower levels are much drier (40–70% relative humidity) due to the location of the town at the southern fringes of the Sahara. The middle levels, however, are relatively moist at the height of the AEJ in the observations (around 80% relative humidity) but not in the model results (around 30% relative humidity). In the model simulation, Tombouctou is located in a region with a sharp moisture gradient at 600 hPa with dry air to the southeast of the station and much moister air to the northwest. At 950 hPa, the station is located at the edge of a region with high AOTs and a low-level convergence to the northwest.

The relation between the dust event and the lower tropospheric moisture can be seen in the radiosoundings in Nouakchott on 9 September at about 23 UTC and the sounding 12 h later (Figure 13). On 9 September at about 23 UTC the relative humidity in the 900 to 700 hPa layer is between 40 and 60% due to the Atlantic Inflow. Twelve hours later, this region is characterized by dry air (relative humidity between 20 and 30%) and high AOTs. At about 600 hPa the relative humidity is high (70–80%), probably due to the altocumulus at the top of the SAL. Strong low-level negative meridional flow (around −14 m s^{-1}) can be observed on 10 September at about 11 UTC, in contrast to the weaker meridional wind 12 h earlier (around −8 m s^{-1}). The differences in the low-level moisture and zonal wind fields in Nouakchott might be related to a slight misplacement of the low-level circulation in the model run and the associated moisture fields.

The comparisons between the COSMO-ART run and satellite images illustrating the atmospheric dust load and the comparison to radiosoundings show that the model represents the atmospheric conditions well and that the model run can be used to analyze the transport of mineral dust toward the developing tropical cyclone Helene.

5. Quantification of Dust Transport Using Trajectories

In this section we will discuss the use of trajectory calculations to determine how the dust reaches the storm from its source regions, where the dust enriched air comes from and where the dry and dust free air northwest of the tropical storm originates. To determine the paths by which the either dry, dry and dusty, or dusty and wet air reaches the tropical storm and its vicinity on 13 September 2006 at 15 UTC, we computed trajectories for different regions. For all the following trajectories, we traced back all air parcels within the selected box.

Forward trajectories were calculated to illustrate how the dust is transported after its emission. The forward trajectories calculated for a box ranging from 16 to 23°N, 14 to 3°W and 5 and 1500 m height on 11 September 2006 at 12 UTC (box A in Figure 14a) show that the moist monsoon flow, which reaches relatively far north that day, moves partly toward the northwest at low levels. Due to the increased surface wind mineral dust is emitted. The dry and dusty air north of 20°N and west of 10°W is mainly transported upward near Cap Blanc to the height of the AEJ and is then transported westward across the Atlantic (Figure 14b). Part of the near-surface, dusty, and moist monsoon flow moves westward and is transported upward into the AEW trough in the coastal baroclinic zone. Some of the trajectories show that air parcels are transported upward to about 200 hPa around 16°W and that this air is relatively moist, dust enriched and probably transported upward by convection which is consistent with the water vapor satellite imagery of this period. The remaining air parcels move northeastward at lower levels and ascend at around 30°N and the Greenwich meridian, lifting dust up to the tropopause. On 13 September 2006 at around 00 UTC, a convective system can be seen in the Meteosat water vapor image in this region (not shown).

Backward trajectories were calculated for regions with maximum mineral dust mass concentration in the northwest (region B, 1500–3000 m, in Figure 15a) and northeast (region C, 2000–4000 m, in Figure 15a) of the tropical storm at around 700 hPa. We can see very nicely in Figure 15b, that the air in region B comes mainly from the AEJ itself which is slightly higher over land than over the ocean due to the weakening of the meridional temperature gradients, and from subsidence in the anticyclone. With relative humidity values below 25% (not shown), the air resulting from subsidence in the subtropical anticyclone is drier than the air that is transported by AEJ, which shows relative humidity values below 50%. The region north-northwest of box B is

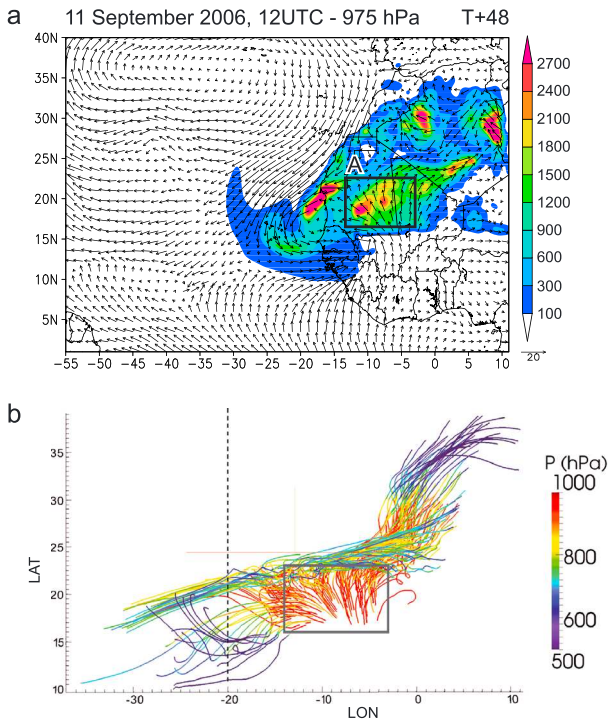

Figure 14. Forward trajectories starting on 11 September 2006 at 12 UTC and ending on 13 September 2006, 15 UTC. The horizontal box A in which the trajectories originate ranges from 16 to 23°N, 14 to 3°W and extends vertically between 5 and 1500 m height. (a) The mineral dust mass concentration (μg m^{-3}) and the horizontal wind field at 975 hPa on 11 September 2006 at 12 UTC is shown as well as the position of the box for which the trajectories were calculated. (b) The pressure (hPa) along the trajectories is displayed in color. A total of 9315 trajectories was computed but only every 50th is displayed. The trajectories are calculated for the model run initialized on 9 September 2006 at 12 UTC. The dashed line indicates the approximate position of the West African coast line.

dry but does not contain mineral dust (Figures 11b, 11d, and 11f). Forward and backward trajectories showed that this dry air is a result of subsidence. Air parcels move anticyclonically around the high pressure system at about 500 hPa and descent while the anticyclone moves westward. As this relatively moist air descends it becomes dryer, i.e., the relative humidity decreases. This nondust related dry air enhances the moisture gradient to the northwest of the developing tropical depression. The air in box B also originates from the dry and dusty north-easterlies and the Harmattan over West Africa, as well as from the moist and dusty monsoon flow that was transported upward over land.

The air in the region with high dust concentrations northeast of the storm's center (region C in Figure 15a), originates partly from the relatively moist (relative humidity larger than 75%) low-level flow on the eastern flank of the anticyclone and also from the relatively dry AEJ (relative vorticity below 50%) (Figure 15c). The trajectories starting in the lower part of box C show that the air in this region originates from the dry and dusty north-easterlies and the Harmattan, as well as the moist and dusty monsoon flow (Figure 15d). When the dust laden, dry air originating over West Africa reaches the monsoon trough, it moves cyclonically around it, the relative humidity increases, and the air is transported upward in the baroclinic zone along the West African coast between 10 and 20°N. The relative humidity of this rising air was relatively high (above 75%). The remaining part comes from air below about 850 hPa that is transported southwestward by the Harmattan. Part of this air mass rotated around the monsoon trough and was transported upward when it reached the coastal baroclinic zone.

Box D was positioned around the tropical depression (Figure 16a) to demonstrate all the pathways that influence the tropical depression. The trajectories from this box, which ranges from 50 to 3400 m in height, highlight the main source regions. At upper levels, the AEJ and the AEW play the most important role (Figure 16b). Only a relatively small number of trajectories originates from the anticyclone at about 500 hPa.

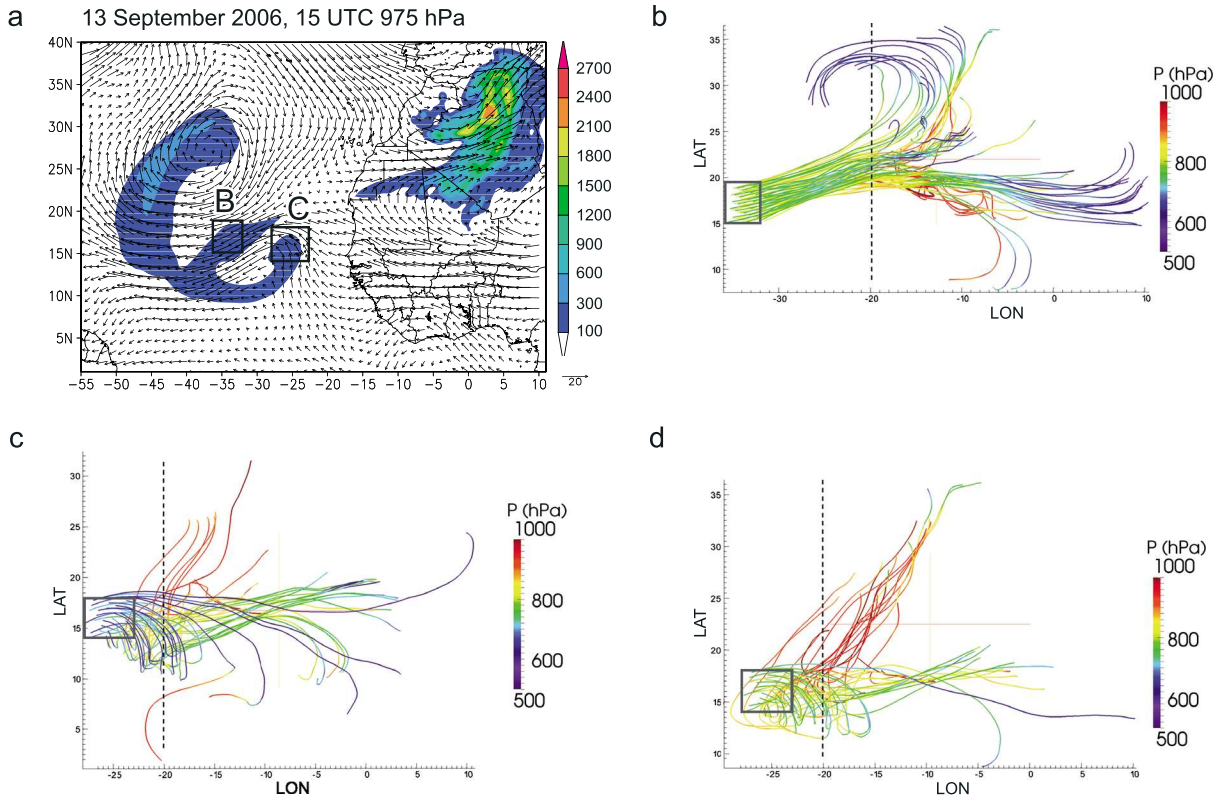

Figure 15. Backward trajectories starting on 13 September 2006 at 15 UTC and ending on 9 September 2006, 18 UTC. The trajectories originate from box B (15–19°N, 36–32°W, 1500–3000 m height) and box C (28–23°W, 14–18°N, 2000–4000 m height). (a) The mineral dust mass concentration (μg m^{-3}) and the horizontal wind field at 700 hPa on 13 September 2006 at 15 UTC are shown as well as the position of the boxes B and C for which the trajectories were calculated. (b) The backward trajectories originating in box B. A total of 1365 trajectories was calculated, but only every 30th is displayed. (c) Trajectories originating in the upper half of box C (3000–4000 m height; a total of 1020 trajectories, but only every 30th is displayed). (d) Trajectories originating in the lower half of box C (2000–3000 m height; a total of 1023 trajectories, but only every 30th is displayed). The pressure (hPa) along the trajectories is displayed in color. The trajectories were calculated for the model run initialized on 9 September 2006 at 12 UTC. The dashed line indicates the approximate position of the West African coast line.

At lower levels, the monsoon flow over the eastern Atlantic, the Harmattan, and the northeasterly trade winds along the West African coast (Figure 16c) have the largest contribution to the air in box D. Fewer trajectories originate in the monsoon flow over land and from the monsoon trough.

The air from the AEJ and the anticyclone is relatively dry. The air from the monsoon flow over land and water is relatively moist, and the air originating from the low-level anticyclone is not as moist as the monsoon flow, but still relatively moist. The Harmattan is dry as expected. These trajectories in combination with the dust distribution previously shown, emphasize that dust is transported by the moist monsoon flow over land, the dry Harmattan and northeasterly trade winds, the relatively dry (below 50% relative humidity at around 800–600 hPa) AEJ, in the moist monsoon trough and by convection.

With the help of the trajectories we could identify the different paths by which the air reached the tropical cyclone. The results are summarized in a schematic shown in Figure 17. Please keep in mind that all weather systems shown here (e.g., the AEW, the anticyclone, and the monsoon trough) move westward with time. This schematic only tries to illustrate where the air masses in and around the tropical storm Helene originate and by which paths the air reaches the storm.

Air at 500 hPa originating over West Africa moves northwestward and then around the anticyclone north of 20°N (path 1 in Figure 17). This air and the air from the anticyclone (path 2 in Figure 17) is descending while moving around the anticyclone. Meanwhile, the relative humidity decreases, which means that the air gets drier. This particularly affects the regions west of the tropical storm at about 700 hPa. At low levels, air from the eastern flank of the anticyclone reaches the storm. Parts of that air reach the low-level monsoon trough

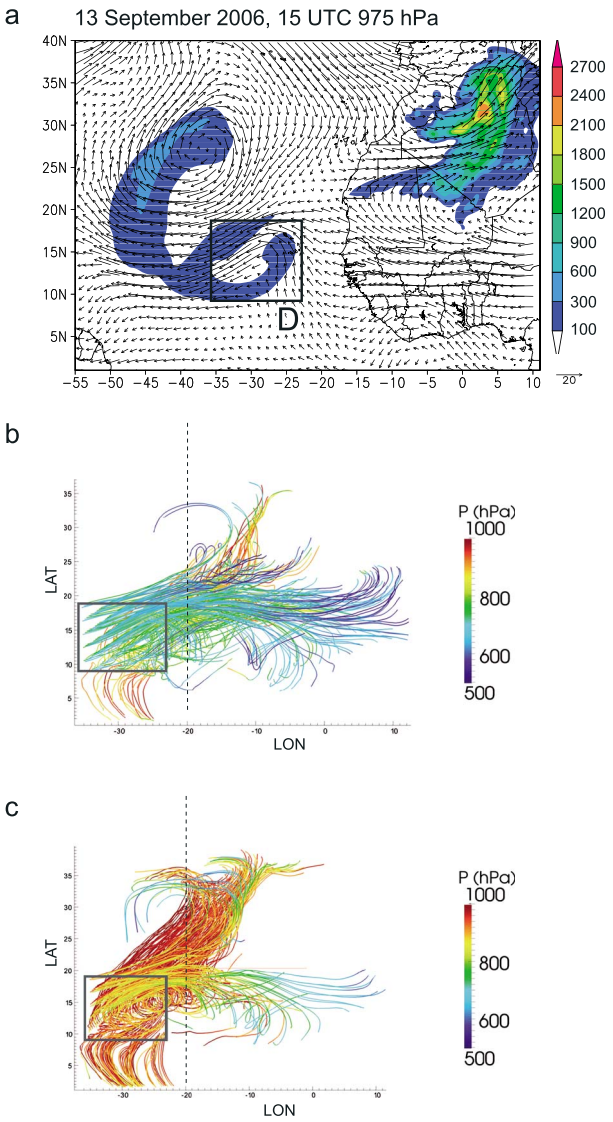

Figure 16. Backward trajectories starting on 13 September 2006 at 15 UTC and ending on 9 September 2006, 18 UTC. The trajectories originate from box D (9–19°N, 36–23°W, 50–4000 m height). (a) The mineral dust mass concentration (μg m^{-3}) and the horizontal wind field at 700 hPa on 13 September 2006 at 15 UTC are shown as well as the position of the box for which the trajectories were calculated. (b) The trajectories for the upper half of the box (2000–4000 m; a total of 12,549 trajectories, but only every 50th is displayed) and (c) the lower half of the box (50–2000 m; a total of 18,827 trajectories but only every 50th is displayed). The pressure (hPa) along the trajectories is displayed in color. The trajectories are calculated for the model run initialized on 9 September 2006 at 12 UTC. The dashed line indicates the approximate position of the West African coast line.

and move cyclonically around it (path 7 in Figure 17). When this air reaches the baroclinic zone along the West African coast between 20 and 10°N, it is transported upward, and when it reaches the height of the AEJ, it is transported westward with it.

Along the West African coast and inland (path 4 in Figure 17) relatively strong north-easterlies occur. They might partly be enhanced by the presence of the anticyclone and due to orographical effects in the lee of the Atlas Mountains in the Western Sahara. This air reaches the low-level circulation, rotates cyclonically around it (along path 7 in Figure 17), and rises upward to the height of the jet when it reaches the baroclinic zone along the coast. A strong Harmattan can also be found over West Africa (path 5 in Figure 17).

During the period analyzed here, the monsoon flow (path 6 in Figure 17) reaches far north and leads to the emission of mineral dust. Parts of the dusty air are transported upward into the trough of the AEW

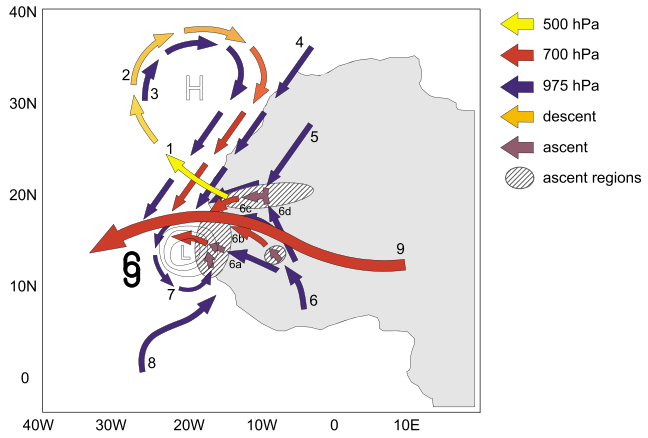

Figure 17. The source regions of air masses reaching tropical storm Helene (2006) and the pathways this air follows are shown. Yellow arrows display the path of air masses around about 500 hPa, red arrows around 700 hPa, and blue arrows display the motion at around 975 hPa. Arrows in shadings of orange depict descent, and ascent is displayed by purple arrows. The regions from which the air in and around the storm originates are as follows: (1) Air at about 500 hPa over West Africa in a region of 15–20°N, 13–20°W. (2) Air in the anticyclone north of 20°N at about 500 hPa that descends as it rotates anticyclonically. (3) Air around the anticyclone at low-levels. (4) Northeasterly trade winds along the West African coast (likely increased by presence of anticyclone and orographical effects on Atlas Mountains) (5) Harmattan over the West African continent. (6) The monsoon flow reaching far north over West Africa. (6a) Southeasterly monsoon flow, which is lifted up in the baroclinic zone along the West African coastline; (6b) southeasterly monsoon flow that is lifted up to the height of the AEW by convection; (6c) southeasterly monsoon flow that stays at lower levels as it moves around the monsoon trough; (6d) south-southeasterly monsoon flow that converges with the Harmattan which leads to ascent of dust. (7) Air in the monsoon trough that moves cyclonically around it. (8) The monsoon flow over the eastern Atlantic that becomes part of the low-level cyclonic circulation. (9) The AEJ that transports relatively dry air at about 700 hPa westward.

by convection, and the dry and dusty air is transported by the AEW (path 6b in Figure 17). Parts of the remaining air move northward where it convergences with the Harmattan (path 6d in Figure 17). Along the ITD, the dust enriched air is transported upward and transported westward by the AEJ. Another path of the monsoon flow is that it moves northwestward into the cyclonic low-level monsoon trough (path 6c in Figure 17). The remaining part moves westward at low-levels and ascends when it reaches the baroclinic zone along the West African coast (path 6a in Figure 17). The lifted air is transported by the AEJ toward the tropical storm. Additionally, the AEJ itself brings air from central Africa toward the storm (path 9 in Figure 17).

The air originating from either the monsoon flow, the north-easterlies, or the low-level anticyclone that reaches the low-level circulation, moves cyclonically around it. The air is then transported upward into the AEW trough and transported toward the storm when it reaches the baroclinic zone along the coast (path 7 in Figure 17). The monsoon flow over the Atlantic (path 8 in Figure 17) enhances the monsoon trough and also rotates cyclonically around it and is partly transported upward when it reaches the baroclinic zone.

6. Summary and Discussion

The aim of this study is to diagnose the properties of the air influencing the cyclogenesis and intensity change of Hurricane Helene (2006) and to describe the transport of mineral dust from its source regions in West Africa toward the developing tropical storm. We consider that a better understanding of the factors that determine the properties of the air that influence a developing tropical cyclones is prerequisite for quantifying the influence of mineral dust on tropical cyclogenesis and intensity change. To do that, we used the model system COSMO-ART, which computes the emission and transport of mineral dust. The advantage of COSMO-ART in the configuration used here is that no dust is contained in the boundary and initial conditions which ensures that all the mineral dust in the simulation is emitted over West Africa. The disadvantage is that the simulation needs to be long enough to allow for the dust to reach the Atlantic and that the dust concentrations are lower than the observed ones as no dust can be advected into the model domain. With the help of COSMO-ART we were able to distinguish between dry, dry and dusty, and wet and dusty regions. Several previous studies

discussed the effect of mineral dust on the development and intensification of tropical cyclones. Some studies [e.g., *Shu and Wu*, 2009] showed that the effect of dust depends on the position of the storm relative to the dust. With the present study, we show how the mineral dust reaches the developing tropical storm.

Between 9 and 14 September 2006, the main source regions of mineral dust were associated with the strong monsoon flow, the strong Harmattan or the north-easterly trade winds, the Atlantic inflow, increased wind speed in the lee of the Atlas Mountains, and north and east of the Hoggar.

The AEW out of which Hurricane Helene developed, the associated weather systems, the mineral dust sources, and the transport of mineral dust were simulated with COSMO-ART. The model results were compared to satellite images illustrating, for instance, the AOT, the SAL, and the total precipitable water. The agreement between the observations and the model results for the whole simulation period was found to be reasonably good, justifying the use of the simulation in this study.

We identified several ways by which the dust laden and dust free air from the different source regions reached the developing tropical storm Helene and its vicinity (Figure 17). Air at 500 hPa originating over West Africa moves northwestward and then around the anticyclone located offshore of the northwestern coast of West Africa. This air is descending while moving around the anticyclone. Meanwhile, the relative humidity decreases. This leads to dry air at about 700 hPa west and northwest of the tropical depression. This is in accordance to *Braun* [2010] who points out that the dry air in the subtropical and eastern Atlantic is often a result of subsidence at the eastern and equatorward side of the Bermuda high-pressure system. However, the anticyclone in our case is on a slightly smaller scale and not the Azores high. At low levels, relatively dry air from the anticyclone partly reaches the storm and partly moves cyclonically around the low-level monsoon trough. When this air reaches the baroclinic zone along the West African coast between 20 and 10°N, it ascends and reaches the height of the AEJ where it is transported westward. Strong north-easterlies along the West African coast and inland reach the low-level circulation, move cyclonically around it and rise upward to the height of the AEJ when this air mass reaches the baroclinic zone along the coast.

The relatively strong and moist monsoon flow reaches far north and leads to the emission of mineral dust. The dust is transported upward into the trough of the AEW by convection and in the coastal baroclinic zone and is then transported westward. Through these processes, relatively moist and dusty air is transported into the trough of the AEW. The remaining low-level air moves northward where it convergences with the Harmattan. Along the ITD, the dust enriched air is transported upward to the height of the AEJ and is then transported westward north of the jet. Another part of the monsoon flow moves northwestward into the low-level monsoon trough. Additionally, the AEJ itself brings air from central Africa toward the storm.

Air originating from the monsoon flow, the northeasterly trade winds, or the low-level anticyclone that reaches the low-level circulation moves cyclonically around it. The air ascends into the AEW trough and is transported toward the storm when it reaches the baroclinic zone along the coast. The monsoon flow over the Atlantic enhances the monsoon trough and also rotates cyclonically around it and is transported upward in the coastal baroclinic zone.

The large amount of mineral dust emitted in the other source regions either reaches the low-level monsoon trough and is then transported as described above or is transported upward at the baroclinic zone along the West African coast or at the ITD and is then transported by the AEJ westward. This dry, dusty, and relatively warm air occurs north of the AEJ.

The trajectories showed that the dry air north and northwest of the tropical storm Helene is indeed partially a result of subsidence in the anticyclone as previously pointed out by *Reale et al.* [2009] and *Braun* [2010]. However, the trajectories also showed that the dry and dusty air that reaches the developing storm is also transported by the AEJ as described by many other studies [e.g., *Dunion and Velden*, 2004; *Karyampudi and Pierce*, 2002]. Additionally, the dust is transported toward Helene by the monsoon flow and the Harmattan. We saw that the dust is not only confined to the regions north of the AEJ but that it can be transported into the AEW trough and into the monsoon trough. The initially dry air becomes moister as it moves around the monsoon trough and may even be transported upward to the height of the AEJ where it is transported westward. Hence, the dusty air is not necessary dry, and thus, it is no SAL, but it might still have an impact on the tropical cyclone's development. This study shows that when analyzing the impact of mineral dust on the development of a tropical depression, it is important to investigate how the dust reaches the storm and where the dust occurs relative to the storm, because dust can be present in both dry and moist regions or dry air can

Acknowledgments
This study was funded primarily through the European Union Integrated Project AMMA. Based on a French initiative, AMMA was built by an international scientific group and was funded by a large number of agencies, of a major financial contribution from the European Community's Sixth Framework Research Programme. Detailed information on scientific coordination and funding is available on the AMMA International web site http://www.ammainternational.org. This work was partly funded by the Feasibility Study of Young Scientists of the Karlsruher Institut für Technologie (KIT). The European Centre for Medium Range Weather Forecast (ECMWF) operational six-hourly analysis data with a horizontal resolution of 0.25° was used to initialize the model. The Meteosat Second Generation (MSG) Spinning Enhanced Visible and Infrared Imager (SEVIRI) imagery is available from http://radagast.nerc-essc.ac.uk/MSG/SEVIRI/DUST/2006/09/. The daily aerosol optical thickness (AOT) fields are obtained from the Moderate Resolution Imaging Spectroradiometer (MODIS)/Aqua Deep Blue Collection 051 over desertic surfaces (MOD08 product) and from MODIS/Terra over the ocean (http://gdata1.sci.gsfc.nasa.gov/daac-bin/G3/gui.cgi?instance_id=MODIS_DAILY_L3). The analyses and visualizations used in this study were produced with the Giovanni online data system, developed and maintained by the NASA GES DISC. We acknowledge the mission scientists and Principal Investigators who provided the data used in this research effort. The attenuated backscatter profile data at 532 nm, retrieved from the spaceborne Cloud-Aerosol Lidar with Orthogonal Polarization (CALIOP) on board the CALIPSO (Cloud-Aerosol Lidar and Infrared Pathfinder Satellite Observation) was obtained from the NASA Atmospheric Science Data Center (https://eosweb.larc.nasa.gov/project/calipso/calipso_table). We are obliged to Jason Dunion and Chris Velden from the Cooperative Institute for Meteorological Satellite Studies (CIMSS) for providing the SAL and the total precipitable water imagery. The lidar measurements of the aerosol concentration on board the NAMMA DC-8 on 12 September 2006 were taken from *Jenkins et al.* [2008]. The radiosonde data are available from the AMMA database (http://database.amma-international.org/). This work benefited from discussions with Jean-Philippe Lafore and John Marsham. We would kindly like to thank Jason Dunion and Gareth Berry for their comments on an earlier version of this manuscript.

be free of dust. A key result from this study is that the route by which dust laden air reaches a tropical cyclone and its vicinity is much more complex than assumed in previous studies. This leads, among other things, to dust being present in regions that are relatively moist, especially in the vicinity of the storm's center.

The main difference to previous studies [e.g., *Dunion and Velden*, 2004] is that dust occurs partly in regions that are relatively moist, especially in the vicinity of the storm's center. If the air is dry and dust enriched, then it is likely to suppress convection as pointed out by several other studies. Our study shows that it is the combination between the dry and dusty air, i.e., SAL, [e.g., *Dunion and Velden*, 2004; *Karyampudi and Pierce*, 2002], the dry but dust free air resulting from subsidence in the anticyclone [*Braun*, 2010], and the dust enriched but relatively moist monsoon flow [e.g., *Marsham et al.*, 2008] that needs to be taken into account when analyzing the effect of dust and dry air on tropical cyclogenesis.

The effect of dust on the tropical cyclogenesis is assumed to depend on the intensity of the dust event, i.e., the mineral dust mass concentrations [e.g., *Reale et al.*, 2009; *Zhang et al.*, 2007]. The dust concentrations for the Helene case were relatively low compared to other mineral dust events in West Africa [e.g., *Slingo et al.*, 2006; *Stanelle*, 2008; *Bou Karam et al.*, 2009a, 2009b; *Flamant et al.*, 2009]. The influence of mineral dust on tropical cyclogenesis of Hurricane Helene remains to be investigated.

Future work needs to include convection-permitting simulations in order to more realistically represent the cyclogenesis of Hurricane Helene and to investigate the effect of dust on the tropical storm. Moreover, further studies are needed to investigate the effect of mineral dust on the dynamics that led to the tropical cyclogenesis and the dynamics of the tropical cyclone. Such studies could include the calculation of potential temperature and potential vorticity budgets. The dust can influence the formation of clouds and should therefore be included in the model cloud microphysics, and the interaction between cloud processes and dust needs to be investigated. Additionally, future studies need to include the effect of wet deposition.

References

Ackermann, I. J., H. Hass, M. Memmesheimer, A. Ebel, F. B. Binkowski, and U. Shankar (1998), Modal aerosol dynamics model for Europe: Development and first application, *Atmos. Environ.*, *32*, 2981–2999.

Alfaro, S. C., and L. Gomes (2001), Modeling mineral aerosol production by wind erosion: Emission intensities and aerosol size distributions in source areas, *J. Geophys. Res.*, *106*, 18,075–18,084.

Bergametti, G., and G. Forêt (2014), Dust deposition, in *Mineral Dust: A Key Player in the Earth System*, edited by P. Knippertz and J.-B. W. Stuut, pp. 179–197, Springer, Netherlands.

Bergametti, G., L. Gomes, E. Remoudaki, M. Desbois, D. Martin, and P. Buat-Ménard (1989), Present transport and deposition patterns of African dusts to the North-Western Mediterranean, in *Paleoclimatology and Paleometeorology: Modern and Past Patterns of Global Atmospheric Transport*, edited by M. Leinen and M. Sarnthein, pp. 227–252, Springer, Netherlands.

Berry, G. J., C. D. Thorncroft, and T. Hewson (2007), African easterly waves during 2004—Analysis using objective techniques, *Mon. Weather Rev.*, *135*, 1251–1267.

Binkowski, F. S., and U. Shankar (1995), The regional particulate matter model 1: Model description and preliminary results, *J. Geophys. Res.*, *100*, 26,191–26,209.

Bou Karam, D., C. Flamant, P. Knippertz, O. Reitebuch, P. Pelon, M. Chong, and A. Dabas (2008), Dust emissions over the Sahel associated with the West African Monsoon inter-tropical discontinuity region: A representative case study, *Q. J. R. Meteorol. Soc.*, *134*, 621–634.

Bou Karam, D., C. Flamant, M. C. T. P. Tulet, J. Pelon, and E. Williams (2009a), Dry cyclogenesis and dust mobilization in the inter tropical discontinuity of the West African monsoon: A case study, *J. Geophys. Res.*, *114*, D05115, doi:10.1029/2008JD010952.

Bou Karam, D., C. Flamant, P. Tullet, J.-P. Chaboureau, A. Dabas, and M. C. Todd (2009b), Estimate of Sahelian dust emissions in the intertropical discontinuity region of the West African monsoon, *J. Geophys. Res.*, *114*, D05115, doi:10.1029/2008JD010952.

Braun, S. A. (2010), Re-evaluating the role of the Saharan air layer in the Atlantic tropical cyclogenesis and evolution, *Mon. Weather Rev.*, *130*, 2007–2037.

Carlson, T. N., and S. G. Benjamin (1980), Radiative heating rates for Saharan dust, *J. Atmos. Sci.*, *37*, 193–213.

Carlson, T. N., and J. M. Prospero (1972), The large-scale movement of Saharan air outbrakes over the northern equatorial Atlantic, *J. Appl. Meteorol.*, *11*, 283–297.

Chatenet, B., B. Marticorena, L. Gomes, and G. Bergametti (1996), Assessing the micro-ped size distribution of desert soils erodible by wind, *Sedimentology*, *43*, 901–911.

Diaz, H. F., T. N. Carlson, and J. M. Prospero (1976), A study of the structure and dynamics of the Saharan air layer over the northern equatorial Atlantic during BOMEX, Tech. Memo. ERL WMPO-32, Natl. Hurricane and Exp. Meteorol. Lab. NOAA, Boulder, Colo.

Doms, G., and U. Schättler (2002), A description of the nonhydrostatic regional model LM. Part I: Dynamics and Numerics, COSMO Doc., Deutscher Wetterdienst, Offenbach, Germany. [Available at www.cosmo-model.org.]

Dunion, J. P. (2011), Rewriting the climatology of the tropical north Atlantic and Caribbean sea atmosphere, *J. Clim.*, *24*, 893–908.

Dunion, J. P., and C. S. Velden (2004), The impact of the Saharan air layer on Atlantic tropical cyclone activity, *Bull. Am. Meteorol. Soc.*, *85*, 353–365.

Flamant, C., J.-P. Chaboureau, D. J. Parker, C. M. Taylor, J.-P. Cammas, O. Bock, F. Timouk, and J. Pelon (2007), Airborne observations of the impact of a convective system on the planetary boundary layer thermodynamics and aerosol distribution in the West African monsoon inter-tropical discontinuity region, *Q. J. R. Meteorol. Soc.*, *133*, 1–28.

Flamant, C., C. Lavaysse, M. C. Todd, J.-P. Chaboureau, and J. Pelon (2009), Multi-platform observations of a representative springtime case of Bodélé and Sudan dust emission, transport and scavenging over West Africa, *Q. J. R. Meteorol. Soc.*, *135*, 413–430.

Grams, C. M., S. C. Jones, J. Marsham, D. J. Parker, J. M. Haywood, and V. Heuveline (2010), The Atlantic inflow to the Saharan heat low: Observations and modelling, *Q. J. R. Meteorol. Soc.*, *136*(s1), 125–140.

Helmert, J., B. Heinold, I. Tegen, O. Hellmuth, and M. Wendisch (2007), On the direct and semidirect effects of Saharan dust over Europe: A modeling study, *J. Geophys. Res.*, *112*, D13208, doi:10.1029/2006JD007444.

Hua, B. L., and P. Klein (1998), An exact criterion for the stirring properties of nearly two-dimensional turbulence, *Phys. D*, *113*, 98–110.

Jacobsen, I., and E. Heise (1982), A new economic method for the computation of the surface temperature in numerical models, *Beitr. Phys. Atmos.*, *55*, 128–141.

Jenkins, G. S., A. S. Pratt, and A. Heymsfield (2008), Possible linkage between Saharan dust and tropical cyclone rain band invigoration in the eastern Atlantic during NAMMA-06, *Geophys. Res. Lett.*, *35*, L08815, doi:10.1029/2008GL034072.

Jones, T. A., D. J. Cecil, and J. Dunion (2007), The environmental and inner-core conditions governing the intensity of Hurricane Erin (2001), *Weather Forecasting*, *22*, 708–2725.

Karyampudi, V. M., and T. Carlson (1988), Analysis and numerical simulations of the Saharan air layer and its effects on easterly wave disturbances, *J. Atmos. Sci.*, *45*, 3102–3136.

Karyampudi, V. M., and H. F. Pierce (2002), Synoptic-scale influence of the Saharan air layer on tropical cyclone genesis over the Eastern Atlantic, *Mon. Weather Rev.*, *130*, 3100–3128.

Karyampudi, V. M., et al. (1999), Validation of the Saharan dust plume conceptual model using lidar, Meteosat, and ECMWF data, *Bull. Am. Meteorol. Soc.*, *80*, 1045–1075.

Kessler, E. (1969), *On the Distribution and Continuity of Water Substance in Atmospheric Circulation Models*, Meteorol. Monogr., vol. 10, Boston, Mass.

Knippertz, P., and A. Fink (2006), Synoptic and dynamic aspects of an extreme springtime Saharan dust outbreak, *Q. J. R. Meteorol. Soc.*, *132*, 1153–1177.

Knippertz, P., C. Deutscher, K. Kandler, T. Müller, O. Schulz, and L. Schütz (2007), Dust mobilization due to density currents in the Atlas region: Observations from the SAMUM 2006 field campaign, *J. Geophys. Res.*, *111*, D21109, doi:10.1029/2007JD008774.

Kocha, C., J.-P. Lafore, P. Tulet, and Y. Seity (2012), High-resolution simulation of a major West African dust-storm: Comparison with observations and investigation of dust impact, *Q. J. R. Meteorol. Soc.*, *138*, 455–470, doi:10.1002/qj.927.

Lu, H., and Y. Shao (1999), A new model for dust emission by saltation bombardment, *J. Geophys. Res.*, *104*, 16,827–16,841.

Mahowald, N., S. Albani, J. F. Kok, S. Engelstaedter, R. Scanza, D. S. Ward, and M. G. Flaner (2014), The size distribution of desert dust aerosols and its impact on the Earth system, *Aeolian Res.*, *15*, 53–717.

Marsham, J. H., D. J. Parker, C. M. Grams, C. M. Taylor, and J. M. Haywood (2008), Uplift of Saharan dust south of the intertropical discontinuity, *J. Geophys. Res.*, *113*, D21102, doi:10.1029/2008JD009844.

Mellor, G. L., and T. Yamada (1974), A hierarchy of turbulent closure models for planetary boundary layers, *J. Atmos. Sci.*, *31*, 1791–1806.

Parker, D. J., R. Burton, A. Diongue-Niang, R. Ellis, M. Felton, C. M. Taylor, C. D. Thorncroft, P. Bessemoulin, and A. Tompkins (2005a), The diurnal cycle of the West African monsoon circulation, *Q. J. R. Meteorol. Soc.*, *131*, 2839–2860.

Parker, D. J., C. D. Thorncroft, R. Burton, and A. Diongue-Niang (2005b), Analysis of the African easterly jet using aircraft observations from the JET2000 experiment, *Q. J. R. Meteorol. Soc.*, *131*, 1461–1482.

Prospero, J. M., and T. N. Carlson (1972), Vertical and areal distributions of Saharan dust over the western equatorial North Atlantic Ocean, *J. Geophys. Res.*, *77*, 5255–5265.

Reale, O., W. K. Lau, K.-M. Kim, and E. Brin (2009), Atlantic tropical cyclogenetic processes during SOP-3 NAMMA in the GEOS-5 global data assimilation and forecast system, *J. Atmos. Sci.*, *66*, 3563–5253.

Redelsperger, J.-L., C. D. Thorncroft, A. Diedhiou, T. Lebel, D. J. Parker, and J. Polcher (2006), African Monsoon, Multidisciplinary Analysis (AMMA): An international research project and field campaign, *Bull. Am. Meteor. Soc.*, *87*, 1739–1746, doi:10.1175/BAMS-87-12-1739.

Ritter, B., and J.-F. Geleyn (1992), A comprehensive radiation scheme for numerical weather prediction models with potential application in climate models, *Mon. Weather Rev.*, *120*, 303–325.

Schepanski, K., I. Tegen, B. Laurent, B. Heinold, and A. Macke (2007), A new Saharan dust source activation frequency map derived from MSG-SEVIRI IR-channels, *Geophys. Res. Lett.*, *34*, L18803, doi:10.1029/2007GL030168.

Schwendike, J. (2010), Convection in an African easterly wave over West Africa an the eastern Atlantic: A model case study of Helene (2006) and its interaction with the Saharan air layer, PhD thesis, Karlsruhe Inst. of Meteorol., Karlsruhe, Germany.

Schwendike, J., and S. C. Jones (2010), Convection in an African easterly wave over West Africa and the eastern Atlantic: A model case study of Helene (2006), *Q. J. R. Meteorol. Soc.*, *136*(s1), 364–396.

Shu, S., and L. Wu (2009), Analysis of the influence of Saharan air layer on tropical cyclone intensity using AIRS/Aqua data, *Geophys. Res. Lett.*, *36*, L09809, doi:10.1029/2009GL037634.

Slingo, A., et al. (2006), Observations of the impact of a major dust storm on the atmospheric radiation balance, *Geophys. Res. Lett.*, *33*, L24817, doi:10.1029/2006GL027869.

Stanelle, T. (2008), Wechselwirkungen von Mineralstaubpartikeln mit thermodynamischen und dynamischen Prozessen in der Atmosphäre über Westafrika, PhD thesis, Institut für Meteorologie und Klimaforschung, Universität/Forschungszentrum Karlsruhe, Karlsruhe, Germany.

Stanelle, T., B. Vogel, H. Vogel, D. Bäumer, and C. Kottmeier (2010), Feedback between dust particles and atmospheric processes over West Africa in March 2006 and June 2007, *Atmos. Chem. Phys. Discuss.*, *10*, 7553–7599.

Sun, D., W. K. M. Lau, M. Kafatos, Z. Boybeyi, G. Leptoukh, C. Yang, and R. Yang (2009), Numerical simulations on the impacts of the Saharan air layer on Atlantic tropical cyclone development, *J. Clim.*, *22*, 6230–6250.

Tiedtke, M. (1989), A comprehensive mass flux scheme for cumulus parameterization in large–scale models, *Mon. Weather Rev.*, *117*, 1779–1800.

Vogel, B., C. Hoose, H. Vogel, and C. Kottmeier (2006), A model of dust transport applied to the Dead Sea area, *Meteorol. Z.*, *6*, 611–624, doi:10.1127/0941-2948/2006/0168.

Vogel, B., H. Vogel, D. Bäumer, M. Bangert, K. Lundgren, R. Rinke, and T. Stanelle (2009), The comprehensive model system COSMO-ART—Radiative impact of aerosol on the state of the atmosphere on the regional scale, *Atmos. Chem. Phys.*, *9*, 8661–8680.

Wernli, H., and H. C. Davies (1997), A Lagrangian-based analysis of extratropical cyclones. I: The method and some applications, *Q. J. R. Meteorol. Soc.*, *123*, 467–489.

Winker, D. M., and B. Hunt (2007), First results from CALIOP, paper presented at 3rd symposium on LIDAR Atmospheric Applications, 87th AMS Annual Meeting, San Antonio, Tex., 15–18 Jan.

Wong, S., and A. E. Dessler (2005), Supression of deep convection over the tropical North Atlantic by the Saharan air layer, *Geophys. Res. Lett.*, *32*, L09808, doi:10.1029/2004GL022295.

Zhang, H., G. M. McFarquhar, S. M. Saleeby, and W. R. Cotton (2007), Impact of Saharan dust as CCN on the evolution of an idealized tropical cyclone, *Geophys. Res. Lett.*, *34*, L14812, doi:10.1029/2007GL029876.